IEEE Access
Multidisciplinary ⋮ Rapid Review ⋮ Open Access Journal

Received 23 May 2023, accepted 2 June 2023, date of publication 7 June 2023, date of current version 14 June 2023.

Digital Object Identifier 10.1109/ACCESS.2023.3283598

RESEARCH ARTICLE

Stability Enhancement of Sulselrabar Electricity System Using Mayfly Algorithm Based on Static Var Compensator and Multi-Band Power System Stabilizer PSS2B

MUHAMMAD RUSWANDI DJALAL, IMAM ROBANDI, AND MOHAMMAD ALMAS PRAKASA
Department of Electrical Engineering, Sepuluh Nopember Institute of Technology, Surabaya 60111, Indonesia

Corresponding author: Imam Robandi (robandi@ee.its.ac.id)

This work was supported in part by the Sepuluh Nopember Institute of Technology through its Indonesian Education Scholarships, and in part by the Higher Education Funding Center (BPPT) Kemendikbudristek and the Education Fund Management Institute (LPDP).

ABSTRACT An additional controller in an electric power system is currently required to increase the system stability, especially when a disturbance occurs. The stability of the multimachine system can be increased by installing a Static Var Compensator (SVC) and Power System Stabilizer (PSS). However, SVC and PSS equipment require precise coordination to determine the optimal location and parameters. This study presents an optimal analysis of SVC coordination with single-band PSS1A and multi-band PSS2B (MB-PSS2B) in the South, Southeast and West Sulawesi (Sulselrabar) electrical systems. An artificial intelligence method based on the Mayfly Optimization Algorithm (MOA) is proposed to optimize the location and parameters of the SVC and PSS. A comparative investigation related to controller parameter optimization from a previous work was used to measure the effectiveness of the MOA based on the Firefly Algorithm (FA) and Particle Swarm Optimization (PSO). Performance analysis using the time-domain simulation method to review the speed deviation response, field voltage response, and rotor angle response for each generator, as well as eigenvalue analysis for each control scheme when there is a change in the load disturbance on generators 1 and 13. The results show an increase in bus voltage from critical to marginal conditions and a decrease in network losses after installing SVC on bus 31 of 40 MW capacity. The application of MB-PSS2B based on the MOA provided an increased damping ratio, optimal speed response, rotor angle, field voltage generator, and eigenvalue system after installing 14 PSS.

INDEX TERMS Stability, SVC, multi-band PSS2B, mayfly optimization algorithm, eigenvalue.

I. INTRODUCTION

The inappropriate utilization of additional equipment in an electric power system for system stabilization can lead to various problems. These problems often arise owing to errors in the equipment, such as incorrect reference signal acquisition or suboptimal equipment parameter values. Modifications aimed at enhancing the speed of an electric power system may result in increased oscillation. If an electric power system has more than one machine or is a multimachine system, the issue becomes more complex [1].

Disturbances in the electric power system can occur as either temporary network outages or dynamic changes in the load. These disturbances can result in system instability, which may manifest as speed, rotor angle, or voltage instability. In general, instability is affected by the initial conditions and magnitude of disturbance [2]. These disturbances directly affect the electrical power. Changes in electrical power have an impact on mechanical power. One of the problems leading to instability is the disparity in the response speed between the rapid electrical power response and comparatively slower

The associate editor coordinating the review of this manuscript and approving it for publication was Nagesh Prabhu.

mechanical power response. As a result of these differences, the system experiences oscillations [3], [4].

An electric power system requires voltage stability; however, changes in load conditions can lead to voltage instability, resulting in both undervoltage and overvoltage conditions. Reactive power compensation is required to maintain stability. Under undervoltage and overvoltage conditions, the power is regulated using Static Var Compensators (SVC) [5]. The SVC component consists of a Thyristor-Controlled Reactor (TCR) and capacitor components. To mitigate disturbances in the form of electric power oscillations, additional equipment such as a conventional Power System Stabilizer (PSS) is commonly employed [6], [7], [8]. The PSS component improves stability limits by reducing generator oscillations [9], [10]. PSS damping refers to the capability of the PSS to produce an electric torque component that aligns with the speed variations [11]. The parameters of the voltage limits, SVC working range, and load variations are crucial and carefully considered, making the problem highly complex. To address this problem, a calculation method was employed to determine the optimal placement of the SVC equipment within the system to ensure maximum performance. Similar to SVC, in PSS, optimal parameter tuning plays a crucial role in effectively utilizing PSS for system stabilization.

Owing to the severe impact of these oscillations, mitigating the system instability is essential for power system planning and operation. Various forms of control can be applied to enhance system stability by utilizing tools such as Flexible AC Transmission Systems (FACTS) [12], [13], Static Synchronous Compensator (STATCOM) [14], [15], SVC [16], [17], [18], and PSS [19], [20]. The enhancement provided by the PSS can effectively mitigate various oscillation modes [14], [21]. The development of a multi-band PSS (MB-PSS) with dual inputs offers a higher level of flexibility and reliability compared to a conventional PSS for different oscillation modes [22], [23]. The MB-PSS was developed based on multiple frequency bands and comprises three correlated bands, each of which targets different oscillation modes. Each band consists of a gain, filter, and limiter [24]. Speed changes and generator active power were used as inputs to the MB-PSS2B [25], [26].

In multimachine systems, the application of SVC significantly affects voltage profiles. Using SVC in multimachine systems increases the voltage stability in 140-bus NPCC systems [27]. This study proposes an adaptive mesh-based algorithm for optimizing the SVC controller parameters. In [28], the implementation of a FACTS device based on Cuckoo Search (CS) in the IEEE 57. The CS algorithm was used to determine the location and size of SVCs. The simulation results show that proper installation location and sizing of the SVC can improve the stability of the multimachine system. An SVC optimization approach based on fuzzy logic increases the voltage profile and reduces SVC capacitance [29]. The results show that the proposed method performs well in reducing the harmonic currents and increasing the system voltage profile. Research [30], discussed the use of SVC to optimize power flow and minimize power loss. In addition, the impact of choosing the location and size of the SVC was discussed.

The application of conventional single-input PSS to multimachine systems also positively affects the system. At the Benghazi North Power Plant of the Libyan General Electric Company, PSS1A is used to dampen the swing mode of the power system from oscillations. The optimal value of the PSS1A parameter was determined using the Particle Swarm Optimization (PSO) technique. The installation of PSS1A can overcome significant disturbances at different operating points and improve the power system stability [31]. In [32], the transient stability of a two-area four-engine system was improved by using PSS1A. The PSS1A parameters were optimized using PSO to increase stability and reduce oscillations. Improved stability was also generated in the IEEE 14-Bus system using PSS1A through optimal parameter optimization [33]. Analysis of system performance using the system participation factor approach and pole placement method for the time-domain behavior of the system after a disturbance occurs.

The small-signal stability of a multimachine power system is increased by applying MB-PSS to suppress Low-Frequency Oscillations (LFOs). This practice can reduce engine speed drift [34]. In [35], the Newton-Raphson method was used to tune the MB-PSS in a power system by considering several operating conditions to test the reliability of the Brazilian south-southeastern Brazilian multimachine system. Evaluation of the installation results showed an increase in the damping ratio of the system. In [36], the MB-PSS design was investigated using a two-area four-engine system. The results show that the performance of the optimized MB-PSS is better than that of the conventional PSS, where the power-angle settling time is reduced. The application of MB-PSS in a single-machine-infinite-bus system was also discussed. Research [37] proposed a systematic approach for tuning MB-PSS. Consequently, the MB-PSS design provides adequate attenuation over a wide rotor mode frequency range (0.01Hz to 4 Hz). This study explored the effectiveness of using conventional tuning guidelines for MB-PSS in a single machine infinite bus (SMIB) testing system.

The combination of SVC-PSS equipment on a multimachine system further enhances the performance of the power system. In [16], a multi-area system, the SVC-PSS application was tested on two generators and dampened the power system oscillations when there was a disturbance. In [38], simulations were carried out on a WSCC 3 engine 9 bus system to demonstrate the effectiveness of PSS and SVC devices in increasing the damping ratio of the system. In [39], another study demonstrated the simultaneous coordinated design of a PSS and SVC as damping controllers in a PSO-based multimachine power system to improve the dynamic stability of the power system. In an SMIB system [40], implementing SVC-PSS-based control increased the attenuation efficiency

of the SMIB. Reference [41] discussed the optimal coordination and optimization of fuzzy controllers to design PSS and STATCOM controllers to obtain greater power system fluctuation attenuation. The results of the analysis demonstrate the effectiveness of the coordinated fuzzy controller in terms of the transient and dynamic stability.

The application of SVC-PSS-based control in this study yielded good results in terms of increasing stability, but the case used was a small system or an example system, not a real system. In addition, the PSS type still uses a single input; however, in its development, the system is increasingly dynamic and requires more complex devices. In a previous study, we discussed the application of a single-input PSS in the South, Southeast and West Sulawesi (Sulselrabar) systems in Indonesia [1]. However, considering the ongoing development of the Sulselrabar system, it is crucial to conduct further analysis to assess its stability. The Sulselrabar system connects several large-load centers. This is our first motivation for proposing a new control scheme based on the SVC and MB-PSS for the Sulselrabar system.

The optimization method used in previous research on PSS optimization was based on the Firefly Algorithm (FA) [1] and Particle Swarm Optimization (PSO) [42]. The FA and PSO methods are swarm intelligence-based optimization methods. Presently, a novel swarm intelligence algorithm known as the Mayfly Optimization Algorithm (MOA) has emerged. According to the benchmarking results, this algorithm demonstrated superior performance compared to both the Firefly Algorithm (FA) and Particle Swarm Optimization (PSO) [43]. In addition, the application of the MOA as an optimization method for power systems has been explored and optimal results have been demonstrated. In [44], MOA was applied to facilitate the coordinated and simultaneous tuning of the parameters of the PSS auxiliary damping controller. In [45], the application of the MOA method was proposed to configure the gain of a PID controller. The aim was to enhance the performance of the three-phase active power filter. Reference [46] discussed an effective method based on the MOA for optimizing the PID parameters of a hydro-turbine governor. This approach aims to improve the performance of the governor system. The superior performance of the MOA method serves as our second motivation for employing it as a technique for optimizing the location and parameters of the SVC and MB-PSS in the Sulselrabar system.

Table 1 summarizes the methodology and findings of various studies that highlight research gaps. In addition, it compares the previous job with the current position. The main contributions of this study are summarized as follows:

1) proposed the installation of an SVC to replace reactive power losses, reduce energy losses, regulate voltage and increase the security of the Sulselrabar system operations.
2) The installation of the MB-PSS2B was proposed to increase the stability of the Sulselrabar system.

TABLE 1. Comparison of existing work to proposed work.

Ref	Controller	Method	Remarks
[27]	SVC	Mesh Adaptive	Optimization of SVC controller parameters on a 140-bus NPCC system
[28]	SVC	Cuckoo Search	Optimization of the installation location and SVC sizing on the IEEE 57 bus system
[29]	SVC	Fuzzy Logic	Optimization of SVC parameters on multimachine systems
[30]	SVC	-	Optimization of SVC installation location and sizing on IEEE 9 bus & 30 Bus systems
[47]	PSS1A	-	Optimization of PSS parameters on multimachine systems
[31]	PSS1A	PSO	Optimization of PSS parameters on the Libyan system
[32]	PSS1A	PSO	PSS parameter optimization for two area four engine system
[33]	PSS1A	-	PSS parameter optimization on IEEE 14-Bus system
[34]	MB-PSS2B	IPSO	Optimization of PSS parameters for multimachine systems
[35]	MB-PSS	-	Optimization of PSS parameters for the South-Southeastern Brazilian multimachine system
[37]	MB-PSS	-	PSS optimization on the SMIB system
[36]	MB-PSS	-	PSS optimization on a four-engine, two-area system
[16]	SVC-PSS	-	Optimization of SVC-PSS parameters on 2 generator systems
[38]	SVC-PSS	-	Optimization of SVC-PSS parameters on the WSCC 3 engine 9 bus system
[39]	SVC-PSS	PSO	Optimization of SVC-PSS parameters for multimachine systems
[40]	SVC-PSS	-	Optimization of SVC-PSS parameters on the SMIB system
[41]	SVC-PSS	Fuzzy Logic	Optimization of SVC-PSS parameters on the SMIB system
The current research	SVC-MB-PSS2B	MOA	Optimization of the installation location and sizing of the SVC-MB-PSS2B on the Sulselrabar system

3) The Mayfly Optimization Algorithm (MOA) method was proposed to optimize the location and parameters of SVC and MB-PSS2B in the Sulselrabar system.
4) Investigate the installation of SVC and MB-PSS2B through Time Domain Simulation and Eigenvalue analysis.

The remainder of this paper is organized as follows: Section II provides an overview of the SVC and PSS mathematical models, formulation of optimization methods, and electric

power systems; Section III describes the research methods; Section IV describes the results of the methods applied; and Section V presents the research conclusions.

II. SYSTEM MODEL

A. GENERATOR MODEL

The synchronous generator linear equation can be written in the matrix model of Equation (1), as shown at the bottom of the page, to make it easier to observe the system response. The inputs included in this equation are changes in the current, speed, and phase angle. Simultaneously, the output results show changes in the voltage and mechanical torque of the generator [48]. v_d and v_q are the Stator Voltage d-q axis, v_F is the Rotor Field Voltage, v_D and v_Q are the Rotor Voltage d-q axis, r is the Stator Resistance, L_d and L_q are Rotor Inductance d-q axis, λ_{q0} and λ_{d0} are the initial flux d-q axis, kMF is the Rotating Magnetic Field, M_D and M_Q are Mutual Inductance, Δi_d and Δi_q are Stator Current d-q axis, Δi_F is Rotor Field Current, Δi_D and Δi_Q are Rotor Current d-q axis, $\Delta\omega$ is Generator Speed Change, and $\Delta\delta$ is generator rotor angle change.

B. EXCITATION MODEL

Changes in the load result in a shift in the operating point of the generator. This is determined by the oscillation frequency and rotor angle before reaching a steady state. The oscillations are fast, but the response of some exciters to overcome these oscillations is not sufficiently quick, leading to the system's response shifting to an unstable area. A short exciter was employed to rapidly enhance the damping of system oscillations in the initial swing condition following a disturbance, with the aim of overcoming the aforementioned issues. This type of exciter can reduce negative damping, which hinders torque attenuation. The equation for the fast exciter is given by Equation (2) [49]:

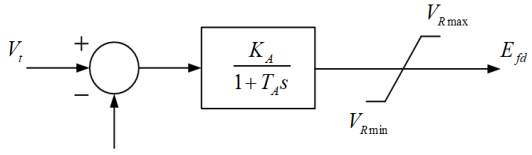

FIGURE 1. Exciter block diagram.

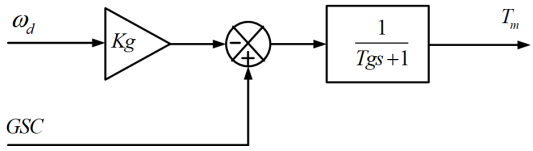

FIGURE 2. Governor modeling.

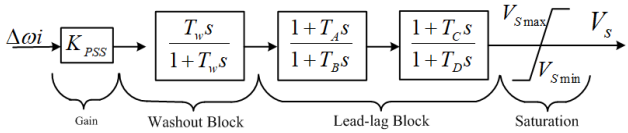

FIGURE 3. Block diagram of PSS1A.

$$E_{fd} = K_A \left(V_t - V_{ref}\right) / \left(1 - T_A s\right) \tag{2}$$

K_A is the gain and T_A is the time constant. Owing to equipment limitations, the output of this exciter must be restricted to within the range of $V_{Rmin} < E_{fd} < V_{Rmax}$. The fast exciter block diagram is shown in Fig. 1.

C. GOVERNOR MODEL

The governor regulates the mechanical torque produced by the generator. Changes in the mechanical torque value (T_m) of the governor are influenced by variations in the speed, load, and speed reference (Governor Speed Changer-GSC). A block diagram of the governor model is shown in Fig. 2 [50].

$$\begin{bmatrix} \Delta v_d \\ -\Delta v_F \\ 0 \\ \Delta v_q \\ 0 \\ \Delta T_m \\ 0 \end{bmatrix} = -\begin{bmatrix} r & 0 & 0 & \omega_0 L_q & \omega_0 kM_Q & \lambda_{q0} & 0 \\ 0 & r_F & 0 & 0 & 0 & 0 & 0 \\ 0 & 0 & r_D & 0 & 0 & 0 & 0 \\ -\omega_0 L_d & -\omega_0 kM_F & -\omega_0 kM_D & r & 0 & -\lambda_{d0} & 0 \\ 0 & 0 & 0 & 0 & r_Q & 0 & 0 \\ \frac{\lambda_{q0} - L_d i_{q0}}{3} & \frac{-kM_F i_{q0}}{3} & \frac{-kM_D i_{q0}}{3} & \frac{-kM_Q i_{d0}}{3} & \frac{kM_Q i_{d0}}{3} & -D & 0 \\ 0 & 0 & 0 & 0 & 0 & -1 & 0 \end{bmatrix} \begin{bmatrix} \Delta i_d \\ \Delta i_F \\ \Delta i_D \\ \Delta i_q \\ \Delta i_Q \\ \Delta\omega \\ \Delta\delta \end{bmatrix}$$
$$- \begin{bmatrix} L_d & kM_F & kM_D & 0 & 0 & 0 & 0 \\ kM_F & L_F & M_R & 0 & 0 & 0 & 0 \\ kM_D & M_R & L_D & 0 & 0 & 0 & 0 \\ 0 & 0 & 0 & L_q & kM_Q & 0 & 0 \\ 0 & 0 & 0 & kM_Q & L_Q & 0 & 0 \\ 0 & 0 & 0 & 0 & 0 & -\tau_j & 0 \\ 0 & 0 & 0 & 0 & 0 & 0 & 1 \end{bmatrix} \begin{bmatrix} \Delta\dot{i}_d \\ \Delta\dot{i}_F \\ \Delta\dot{i}_D \\ \Delta\dot{i}_q \\ \Delta\dot{i}_Q \\ \Delta\dot{\omega} \\ \Delta\dot{\delta} \end{bmatrix} \tag{1}$$

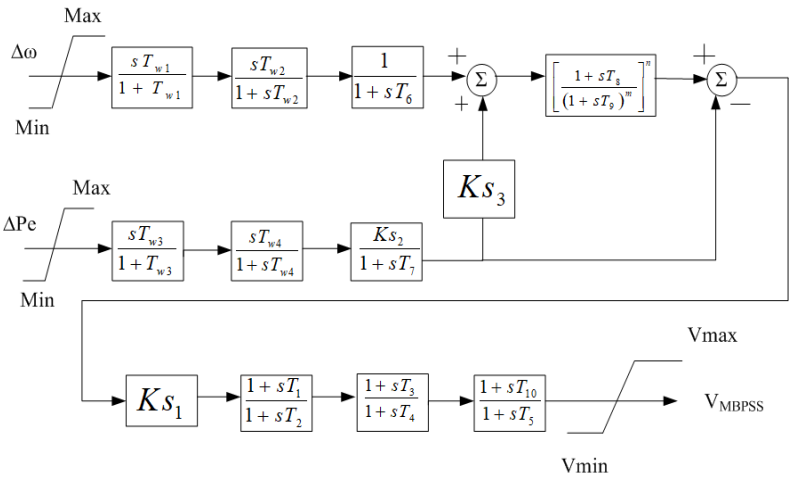

FIGURE 4. Block diagram of MB-PSS2B.

T_m is the mechanical torque, ω_d is the change in speed, *GSC* is Governor Speed Changer (GSC = 0), K_g is Gain Constant (= 1/R), T_g is Governor time constant, R is the droop-governor constant. In this governor model, it was assumed that the GSC was set to 0. The combination of the turbine system with the speed governor generates the mechanical power of the governor, as defined in Equation (3).

$$P_m = -\left[\frac{K_g}{1 + T_g s}\right]\omega_d \tag{3}$$

K_g, T_g, and R represent the gain, governor time, and governor droop constants, respectively. The gain constant and the droop governor constant have an inverse relationship.

D. POWER SYSTEM STABILIZER MODEL

The PSS enhances the damping of the generator electromechanical oscillations. This repair process often entails fluctuations in the speed and power of the generator within a steady-state operating range. The relationship between the aforementioned components is expressed using the swing Equation (4).

$$\frac{2H}{\omega_0}\frac{d^2\delta}{dt} = \bar{T}_m - \bar{T}_e - K_D\Delta\bar{\omega}_r \tag{4}$$

For small disturbances, the above equation becomes:

$$\Delta T_e = T_s\Delta\delta + T_D\Delta\omega \tag{5}$$

δ is the rotor angle, ω is the rotor angular fundamental speed, ω_r is the rotor angular speed, T_m is the mechanical torque, T_e is the electrical torque, H is the inertia constant,, K_D is the damping coefficient, ΔT_e is the change in electric torque, T_s is the synchronization coefficient, T_D is the damping coefficient, $\Delta\delta$ is the change in rotor angle, and $\Delta\omega$ is the change in speed. The PSS model equation is expressed in Equation (6) [51].

$$V_s = K_{pss}\frac{T_w s}{1 + T_w s}\left[\frac{(1 + sT_A)}{(1 + sT_B)}\frac{(1 + sT_C)}{(1 + sT_D)}\right]\omega \tag{6}$$

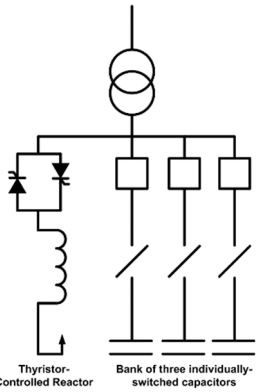

FIGURE 5. One-line diagram of SVC configuration.

V_s is the output PSS, K_{PSS} is the PSS gain, T_w is washout filter, T_A, T_B, T_C, and T_D are lead-lag gains, V_{Smax} and V_{Smin} are limits. A PSS was employed to supply supplementary signals to the generator excitation system, thereby enhancing the damping of the system. Fig. 3 illustrates the modeling of PSS1A [52].

The gain was used as an amplifier to determine the level of attenuation provided by the PSS. The washout function of the PSS introduces a steady-state bias in the PSS output that modifies the generator voltage. The lead-lag compensates for the phase lag introduced by the Automatic Voltage Regulator (AVR) and field-generator circuit. A limiter was used to limit the PSS output.

E. MULTI-BAND POWER SYSTEM STABILIZER MODEL

A Multi-Band Power System Stabilizer (MB-PSS) is a controller device that can reduce signal noise in the power system. This signal effect introduces an input reference error into the system. The noise signal originates from the lateral motion of the shaft, leading to over-modulation of the excitation system. In addition, it can also originate from torsional oscillations resulting from variations in electrical torque. Therefore, noise affects the excitation and electric torque of the generator. MB-PSS was developed from a conventional

single-input PSS to a multi-input PSS. The MB-PSS inputs are the changes in the generator rotor angular velocity ($\Delta\omega$) and generator electrical power (ΔP_e). The input signal was passed through the washout and transducer circuits. The washout circuit ensured a continuous state at the output of the stabilizer, whereas the transducer converted the input signal into a voltage signal. The MB-PSS model was sourced from the IEEE-type PSS2B. The complete MB-PSS model is illustrated in Fig. 4. Each input signal was passed to a washout (T_{w1}-T_{w4}) and transducer (T_6-T_7). The time constants for the torque filters are denoted by T_8 and T_9.

F. STATIC VAR COMPENSATOR

The Static VAR Compensator (SVC) is electrical equipment that compensates for fast-acting reactive power in high voltage electricity transmission networks. SVC is part of the Flexible AC Transmission System (FACTS), which regulates the voltage and stabilizes the system [53]. The term "static" is based on the fact that, when operating or changing the compensation, there are no moving parts of the SVC because the power electronics system controls the compensation process.

If the system power is a capacitive reactive load (leading), the SVC will increase the reactor power to reduce the VAR of the system so that the system voltage drops. In inductively reactive (lagging) conditions, SVC reduces the reactor power to increase the VAR of the system, such that the system voltage increases [54], [55]. In SVC, the amount of VAR and voltage is regulated by adjusting the amount of inductive reactive power compensation in the reactor, while the capacitor bank is static. The location of the SVC can optimize the multimachine system voltage. Fig. 5 shows the SVC configuration.

G. SULSELRABAR SYSTEM

The Sulselrabar system connects the regions of South Sulawesi, Southeast Sulawesi, and West Sulawesi (Sulselrabar). The Sulselrabar system comprises 16 generators and 46 transmission lines that connect the major load centers. The system operates at a voltage of 150 kV and consists of 37 buses. To facilitate the analysis process, bus numbering is required. Table 1 lists the numbers of Sulselrabar electricity system buses.

III. RESEARCH METHOD

This section discusses the comparison and proposed methods for site optimization and the optimal SVC-PSS parameters. In addition, this section describes the implementation of the method using an objective function for optimization. The basic theory behind this method is as follows.

A. OPTIMIZATION TECHNIQUES

The optimization method proposed in this study uses Mayfly Optimization Algorithm (MOA). To validate the MOA method, we used a comparison method employing the Firefly Algorithm (FA) and Particle Swarm Optimization (PSO) with the same objective function. The basic theory behind this method is as described follows.

TABLE 2. Sulselrabar system generation numbering.

Bus	Bus Name	Type	Bus	Bus Name	Type
1	Bakaru	Slack	19	Mamuju	Load
2	Pinrang	Generator	20	Pangkep	Load
3	Pare-Pare	Generator	21	Bosowa	Load
4	Suppa	Generator	22	Tel. Lama	Load
5	Barru	Generator	23	Panakukkang	Load
6	Tello	Generator	24	Tanjung Bunga	Load
7	Tello Lama	Generator	25	Talasa	Load
8	Sgmnsa	Generator	26	TIP	Load
9	Jnpnto	Generator	27	Bone	Load
10	Blkmba	Generator	28	Sidrap	Load
11	Sinjai	Generator	29	Maros	Load
12	Soppeng	Generator	30	Pangkep D	Load
13	Sengkang	Generator	31	Tonasa	Load
14	Makale	Generator	32	Mandai	Load
15	Palopo	Generator	33	Daya	Load
16	Borongloe	Generator	34	TelloA	Load
17	Polmas	Load	35	TelloB	Load
18	Majene	Load	36	Barawaja	Load
			37	Bontoala	Load

1) FIREFLY ALGORITHM [1]

The basic concept of the firefly algorithm is the variation in light intensity and the formula for attraction. The attractiveness of a firefly is defined by the brightness of light intensity $I_{(r)}$, which varies according to the inverse quadrant law [1].

$$I_{(r)} = \frac{I_s}{r^2} \tag{7}$$

I_s is the intensity of the original firefly light, with a fixed light absorption coefficient of γ, and the intensity of light I varies with distance r; then

$$I = I_0 e^{-\gamma r} \tag{8}$$

I_0 is the original light intensity of the firefly. To avoid singularity at $r = 0$ in the expression I_s/r^2, the combined effect of the inverse square law and absorption can be approximated in Gaussian law form.

$$I(r) = I_0 e^{-\gamma r} \tag{9}$$

For a firefly attraction that is proportional to the intensity of light seen by adjacent fireflies, we can determine the attraction β of a firefly at distance r by

$$\beta(r) = \beta_0 e^{-\gamma r^m} \tag{10}$$

β_0 is the attraction at distance $r = 0$. Conversely, for a long scale r during the optimization period, parameter γ can be used as a type of initial value.

$$\gamma = \frac{1}{r^m} \tag{11}$$

Then the distance between every two fireflies i and j on x_i and x_j, respectively, on the Cartesian plane is

$$r_{ij} \left\| x_i - x_j \right\| = \sqrt{\sum_{k=1}^{d} \left(x_{i,k} - x_{j,k} \right)^2} \tag{12}$$

The movement of a firefly attracts other fireflies (lightness), which is determined by

$$x_i = x_i + \beta_0 e^{-\gamma r_{ij}^2}\left(x_j - x_i\right) + \alpha \in_i \tag{13}$$

x_i is the spatial coordination of the I_{th} firefly, x_j is the spatial coordination of the j_{th} firefly, a is the randomization parameter, and $\in_i$ is the vector value of random values between [0-1].

2) PARTICLE SWARM OPTIMIZATION

PSO represents population-based optimization. Several particle populations initially span the problem space in the PSO. Swarms are the names of the scattered particles. The exchange of information between particles allows us to determine which particles are in a position that will produce the best movement-related outcomes. Based on this knowledge, other particles can move there using a velocity motion function. Each particle chooses its position during flight based on its own experience (P_{best}) and that of the other particles (G_{best}). The speed of each particle can be calculated using Equation (14).

$$v_{k+1} = w.v_k + c_1 rand \times \left(P_{best} - x^k\right) + c_2 rand \times \left(G_{best} - x^k\right) \tag{14}$$

Based on the particle velocity, P_{best} and G_{best} can be computed using Equation (14). The most current position can be obtained using Equation (15):

$$x^{k+1} = x^k + v_{k+1}. \quad k = 1, 2 \ldots n \tag{15}$$

For the following terms, X^k is the search point base, X^{k+1} is the search position, V^k is the speed, V^{k+1} is the modified speed, V_{pbest} the speed based on P_{Best}, V_{gbest} the speed based on G_{best}, n is the number of particles in the group, m is the number of members in the particle, p_{best-i} for P_{best} from k, G_{best-i} for G_{best} from group, w is the weight, and c_i is the weight coefficient. The positive constants were c_1 and c_2, and the random numbers were r_1 and r_2.

Based on Equation (16), the iteration function for variable k with weight of inertia (w) is as follows:

$$w\,(k) = w_{max} - \left(\frac{w_{max} - w_{min}}{max.iter}\right) \times k \tag{16}$$

To ensure that all dimensions move simultaneously, the maximum speed is as follows (17). N represents the maximum number of iterations.

$$v^{max} = \frac{\left(x^{max} - x^{min}\right)}{N} \tag{17}$$

3) MAYFLY OPTIMIZATION ALGORITHM

The mayfly is an animal species with a short life span of only 24 h. Mayflies in their flocks were separated into male and female individuals. Male mayflies will always be the strongest, so they will perform better at optimization. These mayfly individuals are similar to those in Particle Swarm Optimization (PSO). Individuals in the mayfly algorithm update their positions based on their current positions, denoted as i(), and speeds, denoted as i() [56]:

$$P_i(t+1) = P_i(t) + v_i(t+1) \tag{18}$$

According to Equation (18), all mayflies update their positions based on their respective speed.

a: MOVEMENTS OF MALE MAYFLIES

During the iteration process, the male mayfly performs exploration and exploitation procedures [56]. Speed is updated based on current fitness value $f(x_i)$ and historical best fitness value on track $f(x_{hi})$.

If $f(x_i) > f(x_{hi})$, the male mayfly will update its speed based on its current speed, the distance between them and the global best position, and the historical best trajectory.

$$v_i\,(t+1) = g.v_i\,(t) + a_i e^{-\beta r_p^2}\left[x_{hi} - x_i\,(t)\right] + a_2 e^{-\beta r_g^2}\left[x_g - x_i(t)\right] \tag{19}$$

The variable g is a linearly descending variable that decreases from the maximum value to the minimum value. This descent is influenced by weight-balancing constants $a1$, $a2$, and β. rp and rg are variables used to determine the Cartesian distance between individuals and their historical best positions in the swarm. In Cartesian space, the second norm is used for distance arrays and can be calculated as:

$$\left|\left|x_i - x_j\right|\right| = \sqrt{\sum_{k=1}^{n}\left(x_{ik} - x_{jk}\right)^2} \tag{20}$$

If $f(x_i) < f(x_{hi})$, the male mayfly will update its speed using a random dance coefficient, denoted as d, from its current speed according to the following equation:

$$v_i(t+1) = g(v_i\,(t) + d.r_i \tag{21}$$

In Equation (21), ri represents a uniformly distributed random number chosen from the domain $[-1, 1]$.

b: MOVEMENTS OF FEMALE MAYFLIES

The speed of the female mayflies was updated using different methods. Biologically, female mayflies with wings have lifespans ranging from one to seven days. Because of this limited time, they exhibited a sense of urgency in finding male mayflies for mating and breeding. Therefore, female mayflies update their speed based on the characteristics and movements of the selected male mayfly [56].

For the i-th female mayfly, if $f(yi) < f(xi)$, the female mayfly will update its speed using the following Equation (22):

$$v_i(t+1) = g.v_i(t) + a_3 e^{-\beta r_{mf}^2}\left[x_i\,(t) - y_i(t)\right] \tag{22}$$

$a3$ is an additional constant that is used to equalize the speed, and rm represents the Cartesian distance between them.

TABLE 3. Algorithm parameters.

Methods	Parameters	Values
FA	Alpha	0.25
	Beta	0.2
	Gamma	1
	Dimension	80
	Number of Firefly	80
	Maximum Iteration	50
PSO	Particles	30
	Most Iterations	50
	The quantity of variables	8
	C2 Social Constant	2
	C1 Cognitive Constant	2
	W Moment Inersia	0.9
MOA	Population Size (males & females)	nPop=20; nPopf=20
	Inertia Weight	g = 0.8
	Inertia Weight Damping Ratio	a1 = 1
	Global Learning Coefficient	$a_2 = 1.5$; $a_3 = 1.5$
	Distance sight Coefficient	Beta = 2
	Nuptial Dance	Dance = 5
	Random flight	fl = 1
	Damping Ratio	dance_damp=0.8
	Mating Parameters	fl_damp=0.99
	Number of Offsprings	nc=20
	Number of Mutants	nm=round(0.05*nPop)
	Mutation Rate	mu=0.01

On the contrary, if $f(yi) < f(xi)$, the female mayfly updates its speed using another random dance coefficient, denoted as fl.

$$v_i(t) = g.v_i(t) + fl.r_2 \tag{23}$$

$r2$ is a randomly generated number chosen from the domain $[-1, 1]$.

c: MATING OF MAYFLIES

All female mayflies and the top half of male mayflies mate, resulting in each pair producing offspring. The offspring inherits traits from their parents and undergoes random evolutionary changes.

$$offspring1 = L * male + (1 - L) * female \tag{24}$$

$$offspring2 = L * female + (1 - L) * male \tag{25}$$

L represents a set of random numbers generated from a Gaussian distribution.

B. OBJECTIVE FUNCTION

This study focused on three main aspects: voltage increase, power flow optimization, and system stability. To achieve increased voltage and power flow optimization, this study focused on optimizing the placement and tuning of the SVC. However, for system stability, this study concentrates on optimizing the placement and tuning of MB-PSS. The system stability performance was analyzed using a time domain simulation method. This method allows for the examination of various responses, such as speed deviation, field voltage (E_{FD}), and rotor angular responses, for each generator. Additionally, eigenvalue analysis was performed to assess the effectiveness of each control scheme. The Eigenvalue analysis method utilizes a mathematical model of the Sulselrabar

TABLE 4. Load flow Sulselrabar system.

Line		Line Losses		Line Losses (SVC)	
From	To	P (MW)	Q (MW)	P (MW)	Q (MW)
1	17	0.877	1.678	0.864	1.632
	2	1.214	2.327	1.191	2.243
2	1	1.214	2.327	1.191	2.243
	3	0.295	-0.282	0.288	-0.309
3	2	0.295	-0.282	0.288	-0.309
	4	0.326	1.060	0.326	1.060
	5	3.529	10.409	3.492	10.279
	17	0.317	-2.469	0.308	-2.502
	20	4.848	15.149	4.898	15.296
	28	0.497	1.505	0.507	1.538
4	3	0.326	1.060	0.326	1.060
5	3	3.529	10.409	3.492	10.279
	20	6.584	21.313	6.623	21.423
6	7	0.048	-0.003	0.048	-0.003
	8	0.002	-0.233	0.002	-0.231
	20	1.805	5.346	1.610	4.633
	21	1.691	4.584	1.475	3.798
	23	1.633	2.987	1.451	2.652
	34	0.195	-0.000	0.199	0.000
	35	0.022	-0.000	0.023	0.000
7	6	0.048	-0.003	0.048	-0.003
	22	0.378	0.000	0.378	0.000
8	6	0.002	-0.233	0.002	-0.231
	24	0.081	0.220	0.081	0.220
	25	0.110	0.133	0.108	0.116
9	29	0.010	-0.726	0.010	-0.726
	10	0.978	2.827	0.961	2.765
	26	0.689	2.113	0.679	2.077
10	9	0.978	2.827	0.961	2.765
	27	0.505	-0.197	0.497	-0.224
11	11	0.281	-0.755	0.276	-0.773
	10	0.281	-0.755	0.276	-0.773
	27	0.775	0.516	0.765	0.478
12	13	1.302	7.025	1.295	6.984
	27	3.067	10.130	3.034	10.011
	28	0.029	-0.855	0.031	-0.847
13	12	1.302	7.025	1.295	6.984
	28	1.703	9.439	1.711	9.487
14	28	0.585	1.122	0.585	1.123
15	15	0.226	0.256	0.226	0.256
15	14	0.226	0.256	0.226	0.256
16	34	0.023	-0.025	0.024	-0.023
17	1	0.877	1.678	0.864	1.632
	3	0.317	-2.469	0.308	-2.502
18	18	0.230	0.107	0.230	0.107
	17	0.230	0.107	0.230	0.107
19	19	0.065	-0.465	0.065	-0.465
	18	0.065	-0.465	0.065	-0.465
20	3	4.848	15.149	4.898	15.296
	5	6.584	21.313	6.623	21.423
	6	1.805	5.346	1.610	4.633
	21	1.425	4.183	1.308	3.739
	30	1.165	0.000	1.271	0.000
21	6	1.691	4.584	1.475	3.798
	20	1.425	4.183	1.308	3.739
22	7	0.378	0.000	0.378	0.000
	37	0.368	0.664	0.368	0.664
23	6	1.633	2.987	1.451	2.652
24	8	0.081	0.220	0.081	0.220
25	8	0.110	0.133	0.108	0.116
	26	0.180	0.805	0.177	0.787
26	9	0.689	2.113	0.679	2.077
	25	0.180	0.805	0.177	0.787
27	10	0.505	-0.197	0.497	-0.224
	11	0.775	0.516	0.765	0.478
	12	3.067	10.130	3.034	10.011
28	3	0.497	1.505	0.507	1.538
	12	0.029	-0.855	0.031	-0.847
	13	1.703	9.439	1.711	9.487
	14	0.585	1.122	0.585	1.123
29	8	0.010	-0.726	0.010	-0.726
	20	1.165	0.000	1.271	0.000

TABLE 4. *(Continued.)* **Load flow Sulselrabar system.**

30	31	0.709	1.293	0.630	1.147
	32	0.868	1.500	0.608	1.022
31	30	0.709	1.293	0.630	1.147
	30	0.868	1.500	0.608	1.022
32	33	0.014	-0.012	0.009	-0.020
	34	0.089	0.101	0.085	0.094
33	32	0.014	-0.012	0.009	-0.020
	34	0.139	0.230	0.139	0.230
	6	0.195	-0.000	0.199	0.000
	16	0.023	-0.025	0.024	-0.023
34	32	0.089	0.101	0.085	0.094
	33	0.139	0.230	0.139	0.230
	35	0.022	0.000	0.023	0.000
	6	0.022	-0.000	0.023	0.000
35	34	0.022	0.000	0.023	0.000
	36	0.000	-0.004	0.000	-0.004
36	35	0.000	-0.004	0.000	-0.004
37	22	0.368	0.664	0.368	0.664
Total		**39.067**	**100.900**	**38.877**	**99.735**

system to analyze the eigenvalues of the system. From the obtained mathematical model, it is converted to a state-space representation using Equations (26) and (27), as follows:

$$\Delta\dot{x} = A\Delta x + B\Delta u \tag{26}$$

$$\Delta y = C\Delta x + D\Delta u \tag{27}$$

System stability can be assessed by examining the eigenvalues of system matrix A, which is an n × n matrix. The state matrix Δx is an n × 1 matrix, the variable output matrix Δy is an m × 1 matrix, and the input variable matrix u is an r × 1 matrix. The system matrix A is an n × n matrix, the input matrix B is an n × r matrix, the measurement matrix C is an m × n matrix, and the direct transmission matrix D is an m × r matrix.

$$\det(\mathrm{sI} - \mathrm{A}) = 0 \tag{28}$$

Equation (29) states that each eigenvalue (λ_i) of matrix A can be represented as a complex number with a real part (σ_i) and an imaginary part ($j\omega_i$), where j represents the imaginary unit. Equation (30) defines the frequency (f) corresponding to the angular frequency (ω) of the eigenvalue. The frequency (f) was obtained by dividing the angular frequency (ω) by 2π. Based on these equations, the number of eigenvalue systems can be determined by analyzing the eigenvalues (λ_i) of matrix A. Each eigenvalue corresponds to a system or mode, and the number of distinct eigenvalues indicates the number of eigenvalue systems.

$$\lambda_i = \sigma_i + j\omega_i \tag{29}$$

$$f = \frac{\omega}{2\pi} \tag{30}$$

The oscillation frequency is given by Equation (30). λ_i is the eigenvalue; σ_i is the real component of the eigenvalue; and ω_i is the imaginary component of the eigenvalue. The real part of the eigenvalues represents the damping component of the system, while the imaginary part represents the oscillation component. Equation (31) represents the damping value.

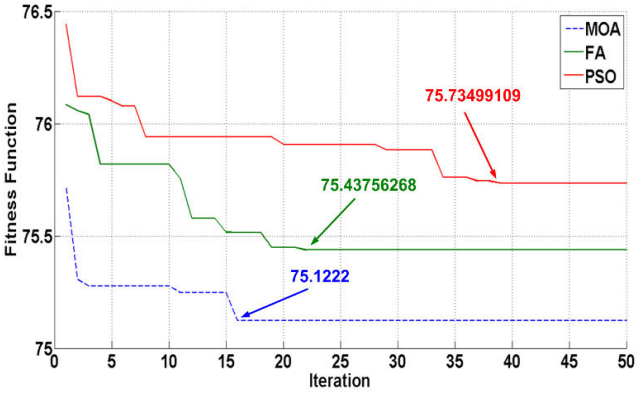

FIGURE 6. Convergence graphic.

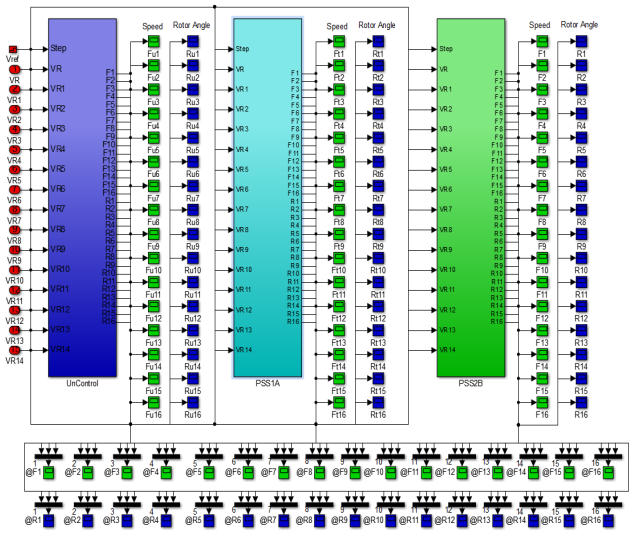

FIGURE 7. System model.

The Comprehensive Damping Index (CDI) value shown in Equation (32) is the overall system attenuation.

$$\zeta_i = \frac{-\sigma_i}{\sqrt{\sigma_i^2 + \omega_i^2}} \tag{31}$$

$$CDI = \sum_{i=1}^{n} (1 - \zeta_i) \tag{32}$$

ζ_i is the damping ratio system and n is the number of eigenvalues. The objective function of the MOA is to maximize the minimum damping ζ_{min}. Equations (33)–(37) are the optimized MB-PSS2B parameter limits.

$$\mathrm{K_{pss(min)}} \le \mathrm{K_{pss}} \le \mathrm{K_{pss(max)}} \tag{33}$$

$$\mathrm{T_{1(min)}} \le \mathrm{T_1} \le \mathrm{T_{1(max)}} \tag{34}$$

$$\mathrm{T_{2(min)}} \le \mathrm{T_2} \le \mathrm{T_{2(max)}} \tag{35}$$

$$\mathrm{T_{3(min)}} \le \mathrm{T_3} \le \mathrm{T_{3(max)}} \tag{36}$$

$$\mathrm{T_{4(min)}} \le \mathrm{T_4} \le \mathrm{T_{4(max)}} \tag{37}$$

Fig. 6 displays the convergence graph, which illustrates the progress of the optimization process using various methods. In the Firefly method, the resulting fitness function value is 75.43756268, and converges in the 22nd iteration. In the PSO method, the resulting fitness function value

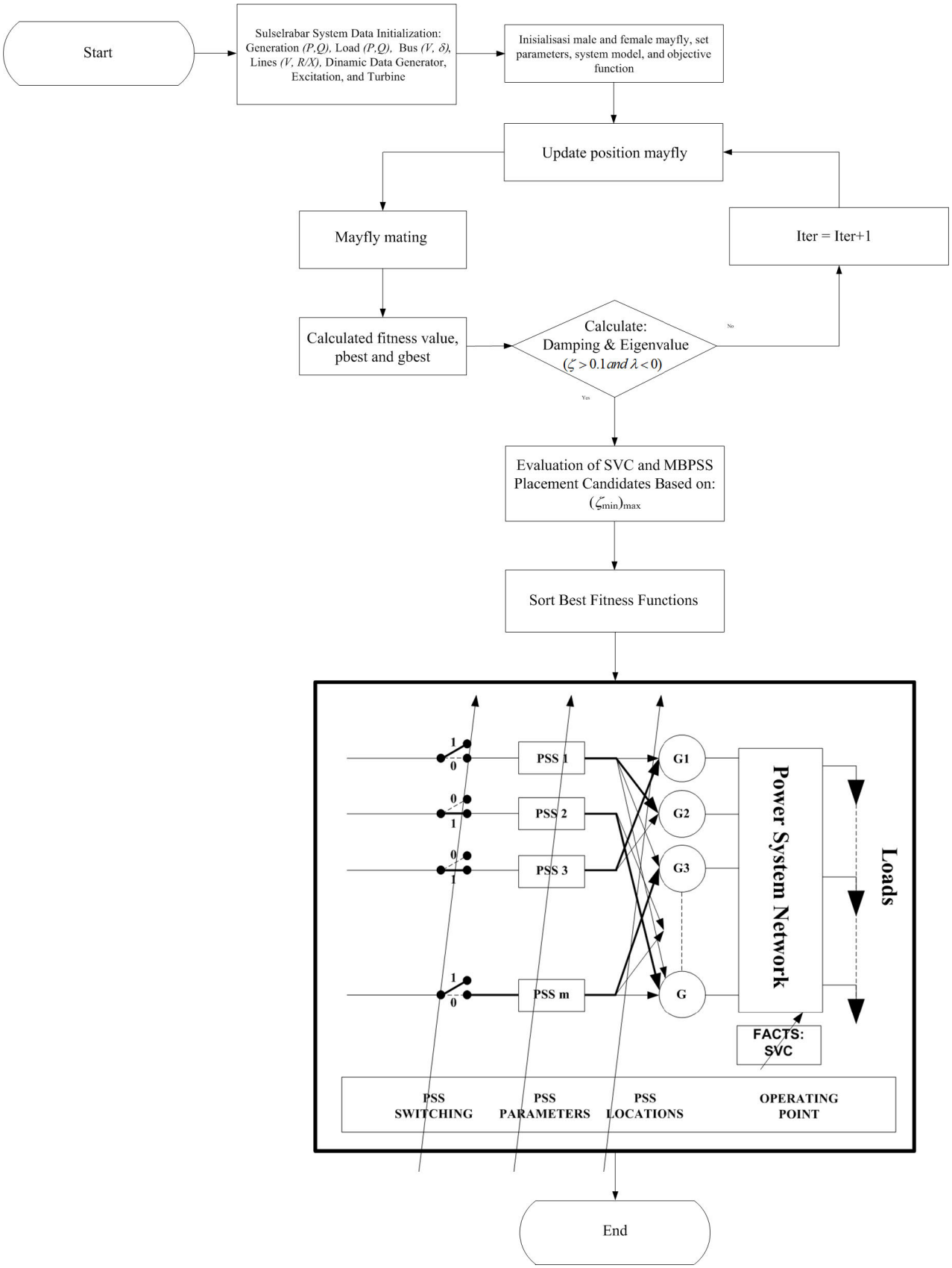

FIGURE 8. Flowchart of research procedures.

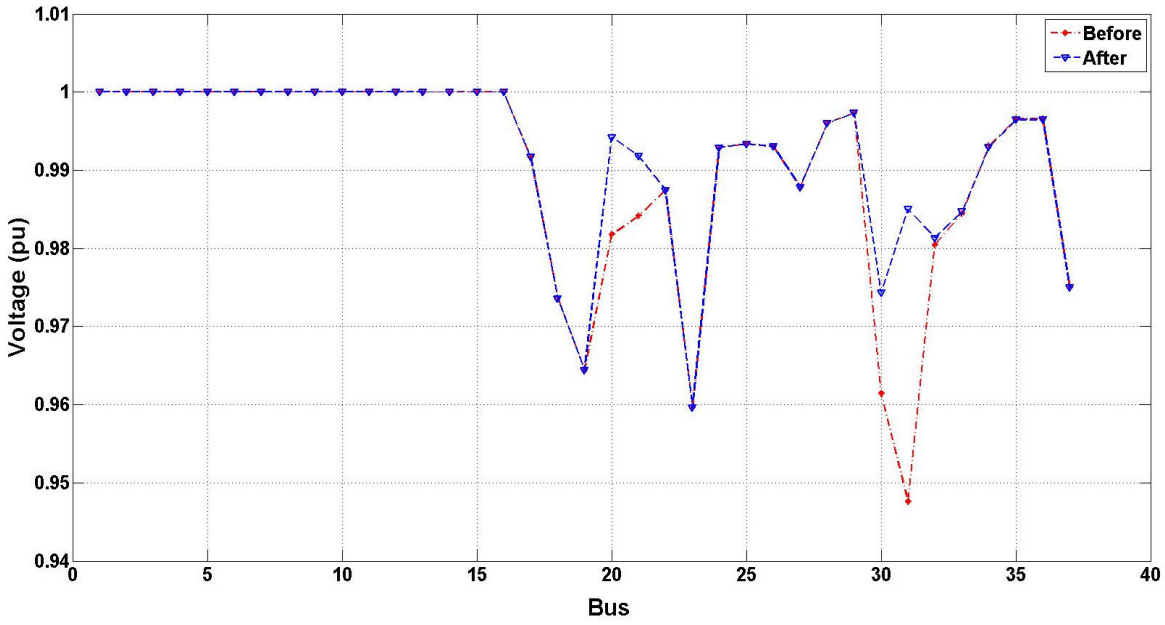

FIGURE 9. Bus voltage profile before and after adding SVC.

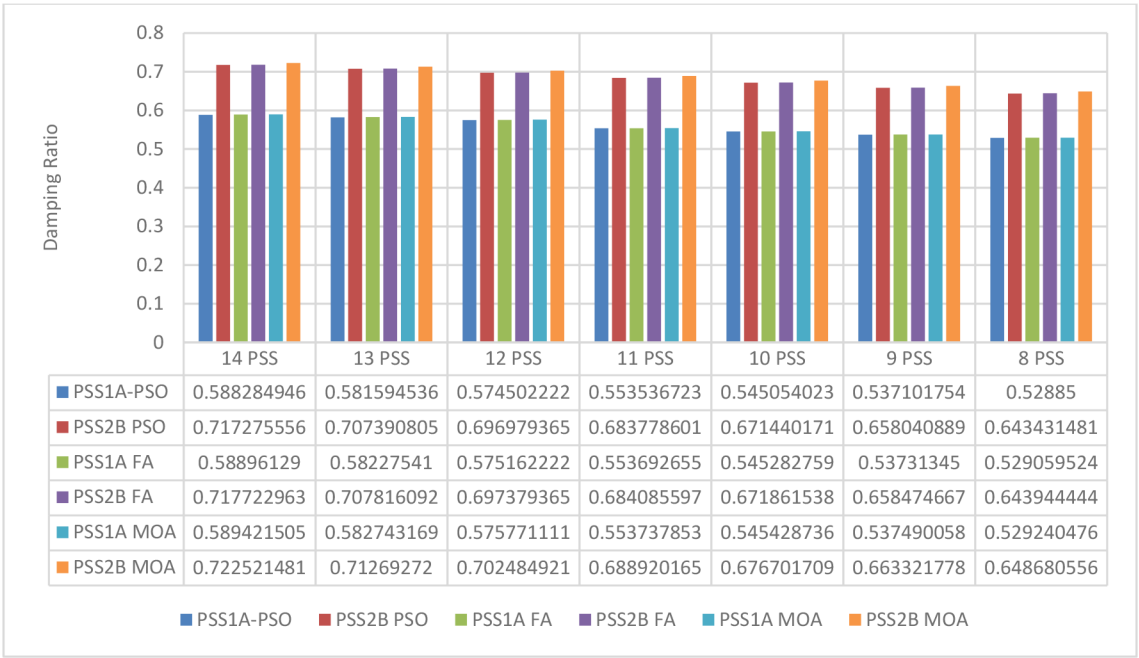

	14 PSS	13 PSS	12 PSS	11 PSS	10 PSS	9 PSS	8 PSS
PSS1A-PSO	0.588284946	0.581594536	0.574502222	0.553536723	0.545054023	0.537101754	0.52885
PSS2B PSO	0.717275556	0.707390805	0.696979365	0.683778601	0.671440171	0.658040889	0.643431481
PSS1A FA	0.58896129	0.58227541	0.575162222	0.553692655	0.545282759	0.53731345	0.529059524
PSS2B FA	0.717722963	0.707816092	0.697379365	0.684085597	0.671861538	0.658474667	0.643944444
PSS1A MOA	0.589421505	0.582743169	0.575771111	0.553737853	0.545428736	0.537490058	0.529240476
PSS2B MOA	0.722521481	0.71269272	0.702484921	0.688920165	0.676701709	0.663321778	0.648680556

FIGURE 10. Placement index damping system.

was 75.73499109, which was achieved at the 39th iteration. In contrast, the method proposed by MOA demonstrated a minimum fitness function value of 75.1222, which was achieved in the 16th iteration. These results suggest that the MOA method achieves a minimum fitness function value in a shorter computational time than the FA and PSO methods do. Table 3 lists the initialization of the method parameters used in this study. Fig. 7 illustrates the system modeling design using the Simulink Model. On the other hand, Fig. 8 demonstrates the optimization procedure employed for parameter tuning and placement of SVC and MB-PSS2B.

IV. RESULTS AND DISCUSSION

A. SVC OPTIMIZATION

The analysis was initiateds by examining the voltage profile and power flow of the Sulselrabar system before the inclusion of the SVC. Table 4 presents the results of the load flow calculations performed using the Newton-Raphson method. In the Sulselrabar system, a shunt capacitor with a rating of 20 Mvar is installed on bus 31. There are 16 generators in the Sulselrabar system. The optimization process for the installation of the SVC was performed on load buses, specifically on 21 buses. The specified range for the SVC

TABLE 5. Tuning results of PSS parameter using firefly algorithm.

G	PSS1A					MB-PSS2B									
	K_{pss}	T_1	T_2	T_3	T_4	K_{pss}	T_1	T_2	T_3	T_4	$Tw_{1\text{-}4}$ Ks_2	T_5	Ks_3 T_7	T_8 T_9	T_{10}
1	27.9260	0.0600	0.9000	0.0500	0.0800	89.4385	145	19	0.4931	0.2000	100	15	1	0.01	0.6
2	10	0.0484	0.3000	0.3931	1.4416	47.6312	129.3956	29.9722	0.2000	1.2000	100	15	1	0.01	0.6
3	10.0401	0.0600	0.3501	0.1000	2.8000	69.6183	84.1928	24.3775	0.2469	1.4515	100	15	1	0.01	0.6
4	16	0.0532	0.8000	0.1323	1.6788	32	129	27.0021	0.3552	1.2003	100	15	1	0.01	0.6
5	33.8670	0.0406	0.3000	0.1456	2.1694	28.0333	94.7643	12.8148	0.5644	0.5000	100	15	1	0.01	0.6
6	36.4233	0.0400	0.4000	0.1000	1.4181	21.6766	76.3757	15.4946	0.1500	0.6735	100	15	1	0.01	0.6
7	30.0266	0.0574	0.0800	0.2000	1.4983	103.1506	76.5673	13	0.5240	0.5041	100	15	1	0.01	0.6
8	37.6188	0.0400	0.0100	0.2000	1.8000	85.4146	130.5288	21.2443	0.2552	0.5145	100	15	1	0.01	0.6
9	10.9864	0.0400	0.8000	0.1000	1.6000	29.6674	145.1560	19.1754	0.4500	0.1453	100	15	1	0.01	0.6
10	40.9630	0.0600	0.9763	0.1876	2.8000	55.9169	117.8609	14.9088	0.3000	0.4200	100	15	1	0.01	0.6
11	98	0.0467	1	0.1978	0.1000	90.8766	124	28.2653	0.0500	0.6500	100	15	1	0.01	0.6
12	9.2352	0.0400	0.3000	0.4092	0.9000	98.4002	92.8414	16.5713	0.4000	0.3446	100	15	1	0.01	0.6
13	10.8342	0.0588	0.1341	0.3000	1.9000	19	129.0038	18.3582	0.4192	0.0892	100	15	1	0.01	0.6
14	17.6793	0.0597	0.3500	0.0163	0.6000	56.6621	78.9859	24	0.4000	0.4461	100	15	1	0.01	0.6

TABLE 6. Tuning results of PSS parameter using particle swarm optimization.

G	PSS1A					MB-PSS2B									
	K_{pss}	T_1	T_2	T_3	T_4	K_{pss}	T_1	T_2	T_3	T_4	$Tw_{1\text{-}4}$ Ks_2	T_5	Ks_3 T_7	T_8 T_9	T_{10}
1	48.4311	0.0600	0.8000	0.0438	0.0900	79.1246	145.7793	17.1953	0.3862	0.1804	100	15	1	0.01	0.6
2	14.4507	0.0400	0.2000	0.3840	1.4614	48.5815	129.1935	29.7339	0.1592	1.1327	100	15	1	0.01	0.6
3	10.0520	0.0542	0.3112	0.1530	2.7000	59.0063	83.0025	23.2334	0.2596	1.5223	100	15	1	0.01	0.6
4	10.0664	0.0469	0.8000	0.2000	1.6175	30.6079	127.2646	27.0048	0.3894	1.2185	100	15	1	0.01	0.6
5	42.3611	0.0574	0.2105	0.2000	2.2000	26.8898	95.8513	13.4176	0.5803	0.4765	100	15	1	0.01	0.6
6	30	0.0600	0.3473	0.1702	1.5000	19.0450	75.3286	15.9049	0.1776	0.6756	100	15	1	0.01	0.6
7	24.5182	0.0418	0.0882	0.1900	1.4611	103.5296	76.8901	13.1154	0.4991	0.5051	100	15	1	0.01	0.6
8	30.9975	0.0400	0.0100	0.1207	1.7063	86.4149	130.4620	20.3835	0.2789	0.5971	100	15	1	0.01	0.6
9	20.8032	0.0577	0.7580	0.1000	1.5000	29.7676	145.1111	18.0504	0.4519	0.1653	100	15	1	0.01	0.6
10	90	0.0523	0.9345	0.1125	2.9000	55.4147	117.7972	14.1784	0.2255	0.3647	100	15	1	0.01	0.6
11	91.2949	0.0600	0.9255	0.2000	0.1000	91.8260	122.2853	28.3063	0.1736	0.6283	100	15	1	0.01	0.6
12	4.8136	0.0516	0.3000	0.4000	0.8263	97.3807	93.2271	16.1421	0.3185	0.2961	100	15	1	0.01	0.6
13	70.9043	0.0470	0.1393	0.4000	2	19.9634	128.7586	17.1513	0.3510	0.0606	100	15	1	0.01	0.6
14	15.5129	0.0496	0.3555	0.0100	0.5000	56.9399	78.3288	24.1062	0.2712	0.4286	100	15	1	0.01	0.6

TABLE 7. Tuning results of PSS parameter using mayfly optimization algorithm.

G	PSS1A					PSS2B									
	K_{pss}	T_1	T_2	T_3	T_4	K_{pss}	T_1	T_2	T_3	T_4	$Tw_{1\text{-}4}$ Ks_2	T_5	Ks_3 T_7	T_8 T_9	T_{10}
1	47.8350	0.0600	0.8839	0.0402	0.0804	120	146	19	0.4000	0.1844	100	15	1	0.01	0.6
2	16.0000	0.0489	0.2218	0.3674	1.4671	68.0727	130.3867	31	0.2000	1.1306	100	15	1	0.01	0.6
3	14.0000	0.0600	0.4000	0.1000	2.7118	110.5575	84.7522	23.9610	0.2102	1.5739	100	15	1	0.01	0.6
4	15.2509	0.0600	0.7729	0.2000	1.7000	61.5223	129	28.4130	0.5000	1.2732	100	15	1	0.01	0.6
5	47.0000	0.0536	0.2000	0.1474	2.1766	67.0301	95.2543	13.2178	0.5864	0.5000	100	15	1	0.01	0.6
6	35.0000	0.0460	0.3998	0.1000	1.4000	61	77	16	0.3000	0.8000	100	15	1	0.01	0.6
7	29.0000	0.0534	0.0800	0.2000	1.4402	184.8315	76.4880	14.8622	0.5178	0.6000	100	15	1	0.01	0.6
8	39.0000	0.0494	0.0100	0.2000	1.7000	116.5679	131.2121	21.9683	0.4000	0.5000	100	15	1	0.01	0.6
9	30.0000	0.0600	0.7244	0.2000	1.5003	50.1994	145	19.2732	0.5400	0.1853	100	15	1	0.01	0.6
10	99.0700	0.0400	0.9151	0.1000	2.8313	95.9051	117.4552	15.0339	0.3000	0.4100	100	15	1	0.01	0.6
11	98.0000	0.0400	0.9000	0.1648	0.1000	161.8771	123.8785	29	0.1454	0.6500	100	15	1	0.01	0.6
12	8.7365	0.0400	0.2000	0.5000	0.8653	168	93.5110	17.8191	0.3099	0.3494	100	15	1	0.01	0.6
13	78.1089	0.0409	0.1400	0.3075	1.9905	50.3194	129.0075	18.8752	0.4254	0.0800	100	15	1	0.01	0.6
14	17.0986	0.0484	0.3552	0.0114	0.6000	86	78	25.9491	0.4000	0.4000	100	15	1	0.01	0.6

TABLE 8. Speed overshoot when interference in bus 1 and bus 13.

G	No PSS (pu)	PSO		FA		MOA	
		PSS1A (pu)	PSS2B (pu)	PSS1A (pu)	PSS2B (pu)	PSS1A (pu)	PSS2B (pu)
G1	-0.0204 & 0.004468	-0.01658 & 0.001971	-0.01341 & 0.001138	-0.01708 & 0.002879	-0.01334 & 0.001321	-0.01623 & 0.002111	-0.01183 & 0.0007239
G2	-0.01958 & 0.005818	-0.01752 & 0.003839	-0.01521 & 0.001093	-0.01727 & 0.003689	-0.01516 & 0.001057	-0.01705 & 0.003518	-0.0138 & 0.0007668
G3	-0.01989 & 0.004673	-0.01853 & 0.00319	-0.01632 & 0.00189	-0.01805 & 0.003587	-0.01625 & 0.001845	-0.018 & 0.003264	-0.01502 & 0.0007891
G4	-0.02008 & 0.005618	-0.01893 & 0.004941	-0.01628 & 0.001035	-0.01818 & 0.004331	-0.01633 & 0.001007	-0.01831 & 0.004527	-0.01468 & 0.0006645
G5	-0.08942 & 0.03744	-0.0715 & 0.01888	-0.05638 & 0.0002752	-0.07509 & 0.0257	-0.05599 & 0.0002774	-0.07016 & 0.01936	-0.04003 & 0.0002057
G6	-0.2175 & 0.05574	-0.2153 & 0.05383	-0.2111 & 0.04836	-0.2146 & 0.05296	-0.211 & 0.04829	-0.2145 & 0.05285	-0.2096 & 0.04747
G7	-0.2069 & 0.08394	-0.1652 & 0.02967	-0.1011 & 0.000357	-0.155 & 0.01837	-0.0998 & 0.0003573	-0.1548 & 0.018	-0.08256 & 0.0005045
G8	-0.05353 & 0.007186	-0.04809 & 0.002788	-0.03946 & 7.761e-05	-0.04615 & 0.0008101	-0.03929 & 7.623e-05	-0.04567 & 0.0004193	-0.03453 & 6.561e-05
G9	-0.02313 & 0.005232	-0.02182 & 0.003833	-0.01964 & 0.001508	-0.0214 & 0.003394	-0.01955 & 0.001401	-0.02138 & 0.00341	-0.01893 & 0.00141
G10	-0.0218 & 0.008538	-0.02037 & 0.007081	-0.0171 & 0.003948	-0.01997 & 0.006746	-0.01711 & 0.003972	-0.01969 & 0.00653	-0.01578 & 0.003202
G11	-0.02315 & 0.01543	-0.02162 & 0.01377	-0.01803 & 0.007068	-0.0213 & 0.01322	-0.01795 & 0.007042	-0.02108 & 0.0132	-0.01638 & 0.005081
G12	-0.02133 & 0.009712	-0.0164 & 0.004138	-0.01635 & 0.003225	-0.0162 & 0.004053	-0.01644 & 0.003211	-0.01605 & 0.00382	-0.01475 & 0.001804
G13	-0.02218 & 0.00455	-0.02168 & 0.003744	-0.01466 & 0.001625	-0.02083 & 0.003648	-0.01456 & 0.001695	-0.02054 & 0.003083	-0.01279 & 0.0009203
G14	-0.02034 & 0.01467	-0.01757 & 0.01086	-0.01591 & 0.007592	-0.01773 & 0.01128	-0.01582 & 0.007445	-0.01717 & 0.01054	-0.0145 & 0.005879
G15	-0.02072 & 0.01624	-0.01875 & 0.01335	-0.01603 & 0.008027	-0.01795 & 0.01243	-0.01593 & 0.007912	-0.0183 & 0.01294	-0.01457 & 0.005857
G16	-0.0635 & 0.01479	-0.05935 & 0.01092	-0.05181 & 0.002905	-0.05811 & 0.009626	-0.05164 & 0.002782	-0.05793 & 0.009466	-0.04894 & 0.002042

TABLE 9. Field voltage response (E_{fd}) when interference in bus 1 and bus 13.

G	No PSS (pu)	PSO		FA		MOA	
		PSS1A (pu)	PSS2B (pu)	PSS1A (pu)	PSS2B (pu)	PSS1A (pu)	PSS2B (pu)
G1	-0.71 & 0.6396	-0.71 & 0.5535	-0.71 & 0.6357	-0.71 & 0.5455	-0.71 & 0.635	-0.71 & 0.5347	-0.71 & 0.634
G2	-0.01472 & 0.03157	-0.01617 & 0.0316	-0.03764 & 0.02936	-0.01559 & 0.03149	-0.04046 & 0.02901	-0.01601 & 0.03129	-0.04737 & 0.02857
G3	-0.05092 & 0.02197	-0.05898 & 0.02159	-0.05854 & 0.02058	-0.05129 & 0.02135	-0.0592 & 0.02036	-0.05918 & 0.02084	-0.07599 & 0.02008
G4	-0.04555 & 0.01956	-0.04615 & 0.01925	-0.05064 & 0.01834	-0.04577 & 0.01908	-0.05143 & 0.01814	-0.046 & 0.01864	-0.05209 & 0.01784
G5	-0.1323 & 0.009718	-0.1299 & 0.009397	-0.1255 & 0.009613	-0.1297 & 0.009186	-0.125 & 0.009602	-0.1289 & 0.008822	-0.1191 & 0.009539
G6	-1 & 9.872e-59	-1 & 1.201e-59	-1 & 1.103e-35	-1 & 0	-1 & 1.103e-35	-1 & 0	-1 & 1.103e-35
G7	-0.925 & 1.006e-58	-0.9009 & 1.256e-59	-0.7773 & 1.103e-35	-0.8899 & 4.63e-61	-0.7721 & 1.103e-35	-0.8889 & 0	-0.7573 & 0.05063
G8	-2.42 & 0.004785	-2.353 & 0.003057	-2.183 & 0.004823	-2.301 & 0.002719	-2.178 & 0.004822	-2.276 & 0.001975	-2.026 & 0.004841
G9	-0.1659 & 0.1321	-0.1688 & 0.1264	-0.1627 & 0.1171	-0.1708 & 0.1219	-0.1626 & 0.117	-0.1756 & 0.1176	-0.1625 & 0.1009
G10	-0.06409 & 0.08074	-0.02037 & 0.007081	-0.06496 & 0.09472	-0.01997 & 0.006746	-0.06498 & 0.09502	-0.01969 & 0.00653	-0.06512 & 0.1028
G11	-0.02736 & 0.02889	-0.02162 & 0.01377	-0.02748 & 0.02868	-0.0213 & 0.01322	-0.02756 & 0.02865	-0.02108 & 0.0132	-0.02742 & 0.02847
G12	-0.1491 & 0.2039	-0.0164 & 0.004138	-0.1664 & 0.2008	-0.0162 & 0.004053	-0.1661 & 0.2008	-0.01605 & 0.00382	-0.1713 & 0.1998
G13	-0.4172 & 0.1344	-0.02168 & 0.003744	-0.4173 & 0.1408	-0.02083 & 0.003648	-0.4173 & 0.1412	-0.02054 & 0.003083	-0.4173 & 0.1426
G14	-0.05658 & 0.05532	-0.01757 & 0.01086	-0.06094 & 0.05566	-0.01773 & 0.01128	-0.06039 & 0.05567	-0.01717 & 0.01054	-0.06431 & 0.05584
G15	-0.02161 & 0.01871	-0.01875 & 0.01335	-0.02105 & 0.02008	-0.01795 & 0.01243	-0.02138 & 0.01999	-0.0183 & 0.01294	-0.02021 & 0.02136
G16	-0.5285 & 7.839e-60	-0.5256 & 1.31e-60	-0.505 & 7.596e-37	-0.5234 & 8.084e-61	-0.5041 & 7.596e-37	-0.5231 & 0	-0.4959 & 7.596e-37

TABLE 10. Rotor angle settling time respon when interference in bus 1 and 13.

G	No PSS (s)	PSO		FA		MOA	
		PSS1A (s)	PSS2B (s)	PSS1A (s)	PSS2B (s)	PSS1A (s)	PSS2B (s)
G1	14.26	11.83	8.55	11.24	8.21	10.25	7.46
G2	14.78	12.25	9.16	11.6	8.52	11.91	6.69
G3	16.46	13.38	9.27	12.9	8.84	12.74	7.25
G4	13.98	11.46	9.77	11.08	8.95	10.79	7.06
G5	12.96	11.61	7.53	11.58	5.71	10.61	5.56
G6	5.41	5.24	4.81	5.2	4.53	5.13	4.65
G7	6.69	6.4	5.6	6.02	5.21	5.88	4.91
G8	10.39	9.16	6.78	8.63	6.12	7.3	5.72
G9	15.79	14.16	10.3	13.58	9.06	12.52	8.45
G10	16.49	13.22	10.17	12.9	9.51	12.79	8.33
G11	13.15	11.76	9.64	11.28	8.63	10.4	6.11
G12	14.16	13.45	11.44	13.27	10.69	12.96	8.91
G13	15.12	13.43	9.75	12.76	8.84	12.07	6.68
G14	16.46	13.9	11.931	12.76	11.45	13.27	10.61
G15	14.78	13.79	12.07	12.93	11.76	12.6	9.97
G16	7.55	7.05	6.77	6.93	5.02	5.901	4.14

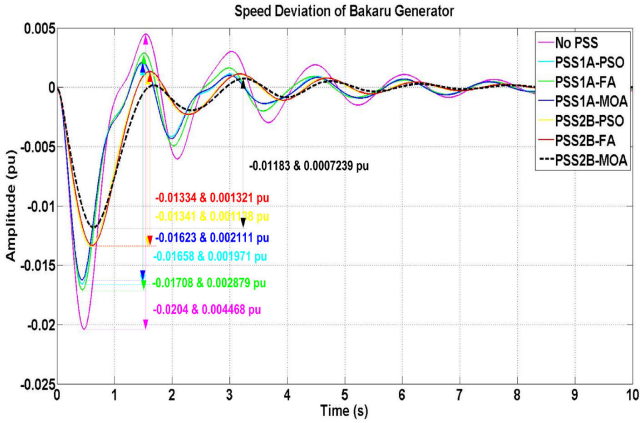

FIGURE 11. Speed deviation ($\Delta\omega$) of Bakaru generator.

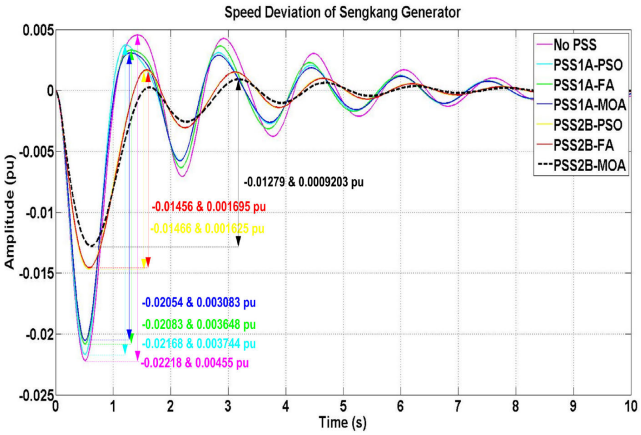

FIGURE 12. Speed deviation ($\Delta\omega$) of Sengkang generator.

installation capacitance was from 0 to 80 Mvar. Table 4 displays the initial profile of the Sulselrabar system before installation of the SVC. The obtained power flow calculation results, indicate that several bus voltage profiles are in marginal and critical condition. According to the system operating standards, the minimum bus voltage should not fall below -5% of the rated voltage. Based on the table, buses 30 and 31 experience marginal and critical conditions, respectively. The marginal voltage condition at bus 30 was 0.9615 pu, whereas the critical voltage condition at bus 31 was 0.9476 pu. When considering the losses without the SVC, the obtained active power (P) was 39.067 MW and the reactive power (Q) was 100.900 MVar. However, with the implementation of SVC, the active power was reduced to 38.877 MW, and the reactive power decreased to 99.735 MVar.

Fig. 7 shows the bus voltage profile of the Sulselrabar system after optimizing the installation of SVC. Based on the analysis results, the optimal location for installing the SVC was determined to be bus 31 with a capacity of 40 MVar. Following the installation of SVC, an increase in the bus voltage profile was observed.

B. MB-PSS2B OPTIMIZATION

In this study, two case studies were conducted to assess the system stability: load change disturbances on the BAKARU and SENGKANG generators. Data processing was performed using MATLAB M-files, whereas system modeling was performed using Simulink MATLAB. The results of the voltage magnitude analysis were derived from a the power flow study conducted after optimizing the Sulselrabar system by including a Static Var Compensator (SVC). Subsequently, the network admittance matrix was reduced, and the obtained results were utilized for the system simulation. The system simulation involved multiple models, including systems without a PSS, PSS1A, and MB-PSS2B. Simulations without a PSS were specifically performed to determine the eigenvalues

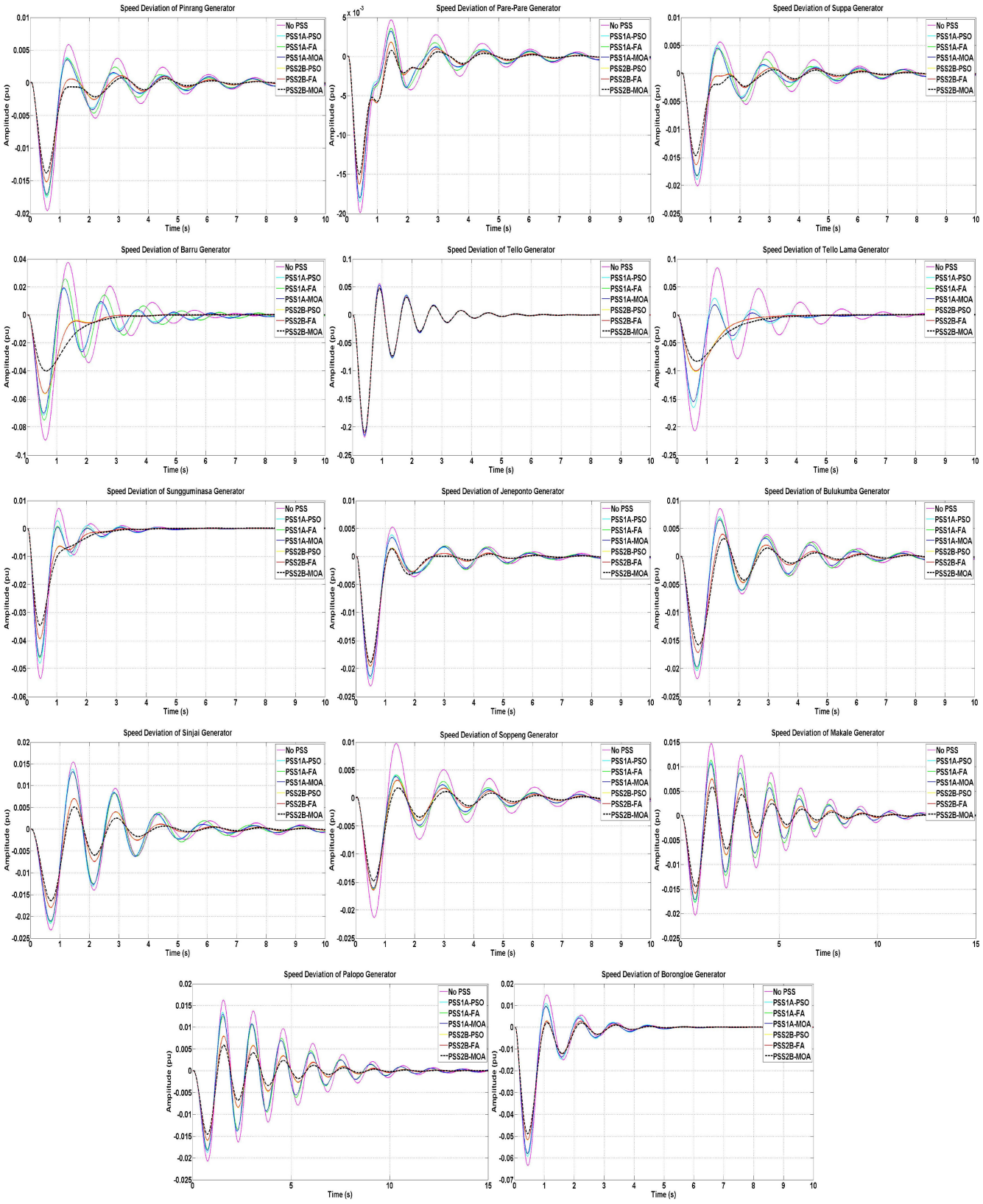

FIGURE 13. Speed deviation ($\Delta\omega$) of all generator.

of the system, which provided insight into the stability of the system. The objective was to observe an increase in system damping, indicating improved stability. By conducting simulations without a PSS and analyzing the system eigenvalues,

TABLE 11. Critical eigenvalue system.

No PSS (pu) 1.0e+02	PSO		FA		MOA	
	PSS1A (pu) 1.0e+02	PSS2B (pu) 1.0e+02	PSS1A (pu) 1.0e+02	PSS2B (pu) 1.0e+02	PSS1A (pu) 1.0e+02	PSS2B (pu) 1.0e+02
-0.5209 + 6.5554i	-0.4588 + 5.1195i	-0.5173 + 6.5583i	-0.4560 + 5.1207i	-0.5170 + 6.5597i	-0.4525 + 5.1220i	-0.5162 + 6.5602i
-0.5209 - 6.5554i	-0.4588 - 5.1195i	-0.5173 - 6.5583i	-0.4560 - 5.1207i	-0.5170 - 6.5597i	-0.4525 - 5.1220i	-0.5162 - 6.5602i
-0.4444 + 5.3203i	-0.3063 + 4.6948i	-0.4425 + 5.3053i	-0.3062 + 4.6947i	-0.4425 + 5.3048i	-0.3062 + 4.6949i	-0.4422 + 5.3015i
-0.4444 - 5.3203i	-0.3063 - 4.6948i	-0.4425 - 5.3053i	-0.3062 - 4.6947i	-0.4425 - 5.3048i	-0.3062 - 4.6949i	-0.4422 - 5.3015i
-0.4144 + 5.0621i	-0.3220 + 4.5384i	-0.4085 + 5.0528i	-0.3208 + 4.5394i	-0.4082 + 5.0524i	-0.3193 + 4.5401i	-0.4066 + 5.0502i
-0.4144 - 5.0621i	-0.3220 - 4.5384i	-0.4085 - 5.0528i	-0.3208 - 4.5394i	-0.4082 - 5.0524i	-0.3193 - 4.5401i	-0.4066 - 5.0502i
-0.3056 + 4.6945i	-0.2225 + 4.5116i	-0.3059 + 4.6956i	-0.2189 + 4.5154i	-0.3058 + 4.6953i	-0.2132 + 4.5199i	-0.3062 + 4.6970i
-0.3056 - 4.6945i	-0.2225 - 4.5116i	-0.3059 - 4.6956i	-0.2189 - 4.5154i	-0.3058 - 4.6953i	-0.2132 - 4.5199i	-0.3062 - 4.6970i
-0.3139 + 4.5323i	-0.0412 + 3.9001i	-0.3219 + 4.5280i	-0.0926 + 4.1568i	-0.3230 + 4.5272i	-0.1366 + 4.3431i	-0.3242 + 4.5267i
-0.3139 - 4.5323i	-0.0412 - 3.9001i	-0.3219 - 4.5280i	-0.0926 - 4.1568i	-0.3230 - 4.5272i	-0.1366 - 4.3431i	-0.3242 - 4.5267i
-0.1972 + 4.4653i	-0.0920 + 4.1558i	-0.1923 + 4.4488i	-0.1378 + 4.3419i	-0.1918 + 4.4476i	-0.1965 + 4.3137i	-0.1907 + 4.4437i
-0.1972 - 4.4653i	-0.0920 - 4.1558i	-0.1923 - 4.4488i	-0.1378 - 4.3419i	-0.1918 - 4.4476i	-0.1965 - 4.3137i	-0.1907 - 4.4437i
-0.1280 + 4.3272i	-0.1385 + 4.3402i	-0.1341 + 4.2886i	-0.1966 + 4.3137i	-0.1355 + 4.2846i	-0.0925 + 4.1576i	-0.1371 + 4.2800i
-0.1280 - 4.3272i	-0.1385 - 4.3402i	-0.1341 - 4.2886i	-0.1966 - 4.3137i	-0.1355 - 4.2846i	-0.0925 - 4.1576i	-0.1371 - 4.2800i
-0.0857 + 4.1565i	-0.1966 + 4.3137i	-0.1968 + 4.3143i	-0.2625 + 4.1931i	-0.1968 + 4.3144i	-0.2624 + 4.1930i	-0.1970 + 4.3149i
-0.0857 - 4.1565i	-0.1966 - 4.3137i	-0.1968 - 4.3143i	-0.2625 - 4.1931i	-0.1968 - 4.3144i	-0.2624 - 4.1930i	-0.1970 - 4.3149i
-0.1965 + 4.3135i	-0.2617 + 4.1921i	-0.2758 + 4.2103i	-0.0412 + 3.9001i	-0.2765 + 4.2113i	-0.0412 + 3.9001i	-0.2810 + 4.2178i
-0.1965 - 4.3135i	-0.2617 - 4.1921i	-0.2758 - 4.2103i	-0.0412 - 3.9001i	-0.2765 - 4.2113i	-0.0412 - 3.9001i	-0.2810 - 4.2178i
-0.2608 + 4.1907i	-0.0821 + 4.0453i	-0.0412 + 3.9001i	-0.0822 + 4.0454i	-0.0412 + 3.9001i	-0.0823 + 4.0456i	-0.0412 + 3.9001i
-0.2608 - 4.1907i	-0.0821 - 4.0453i	-0.0412 - 3.9001i	-0.0822 - 4.0454i	-0.0412 - 3.9001i	-0.0823 - 4.0456i	-0.0412 - 3.9001i
-0.0413 + 3.9001i	-0.0371 + 3.5623i	-0.0369 + 4.1092i	-0.0372 + 3.5626i	-0.0284 + 4.0988i	-0.0372 + 3.5626i	-0.0172 + 4.0844i
-0.0413 - 3.9001i	-0.0371 - 3.5623i	-0.0369 - 4.1092i	-0.0372 - 3.5626i	-0.0284 - 4.0988i	-0.0372 - 3.5626i	-0.0172 - 4.0844i
-0.0821 + 4.0450i	-0.0960 + 2.3024i	-0.0815 + 4.0456i	-0.0926 + 2.3016i	-0.0815 + 4.0456i	-0.0931 + 2.3017i	-0.0813 + 4.0462i
-0.0821 - 4.0450i	-0.0960 - 2.3024i	-0.0815 - 4.0456i	-0.0926 - 2.3016i	-0.0815 - 4.0456i	-0.0931 - 2.3017i	-0.0813 - 4.0462i
-0.0371 + 3.5630i	1.6947 + 0.0000i	-0.0380 + 3.5614i	1.6960 + 0.0000i	-0.0380 + 3.5614i	1.6958 + 0.0000i	-0.0376 + 3.5573i
-0.0371 - 3.5630i	-0.1179 + 1.3750i	-0.0380 - 3.5614i	-0.1187 + 1.3762i	-0.0380 - 3.5614i	-0.1188 + 1.3768i	-0.0376 - 3.5573i
-0.0997 + 2.3039i	-0.1179 - 1.3750i	-0.0394 + 2.2884i	-0.1187 - 1.3762i	-0.0363 + 2.2877i	-0.1188 - 1.3768i	-0.0175 + 2.2824i
-0.0997 - 2.3039i	-0.0032 + 0.0414i	-0.0394 - 2.2884i	-0.0032 + 0.0414i	-0.0363 - 2.2877i	-0.0032 + 0.0414i	-0.0175 - 2.2824i
1.6985 + 0.0000i	-0.0032 - 0.0414i	1.6888 + 0.0000i	-0.0032 - 0.0414i	1.6886 + 0.0000i	-0.0032 - 0.0414i	1.6695 + 0.0000i
-0.1487 + 1.5168i	-0.0043 + 0.0463i	-0.1448 + 1.5122i	-0.0044 + 0.0479i	-0.1446 + 1.5120i	-0.0043 + 0.0463i	-0.1418 + 1.5091i
-0.1487 - 1.5168i	-0.0043 - 0.0463i	-0.1448 - 1.5122i	-0.0044 - 0.0479i	-0.1446 - 1.5120i	-0.0043 - 0.0463i	-0.1418 - 1.5091i
-0.1171 + 1.3752i		-0.1110 + 1.3699i	-0.0043 + 0.0463i	-0.1127 + 1.3710i		-0.1044 + 1.3640i
-0.1171 - 1.3752i		-0.1110 - 1.3699i	-0.0043 - 0.0463i	-0.1127 - 1.3710i		-0.1044 - 1.3640i
-0.0033 + 0.0409i		-0.0054 + 0.0674i		-0.0054 + 0.0670i		0.0056 + 0.0655i
-0.0033 - 0.0409i		-0.0054 - 0.0674i		-0.0054 - 0.0670i		0.0056 - 0.0655i
-0.0044 + 0.0462i		-0.0039 + 0.0410i		-0.0039 + 0.0409i		
-0.0044 - 0.0462i		-0.0039 - 0.0410i		-0.0039 - 0.0409i		

TABLE 12. Inter-area eigenvalue system.

No PSS (pu) 1.0e+02	PSO		FA		MOA	
	PSS1A (pu) 1.0e+02	PSS2B (pu) 1.0e+02	PSS1A (pu) 1.0e+02	PSS2B (pu) 1.0e+02	PSS1A (pu) 1.0e+02	PSS2B (pu) 1.0e+02
-0.3305 + 4.0946i	-0.5904 + 4.9911i	-2.8014 + 3.6518i	-0.3205 + 4.1403i	-3.0139 + 4.7198i	-0.5206 + 5.0016i	-4.1030 + 2.7373i
-0.4444 + 4.6227i	-0.3218 + 4.1411i	-1.7172 + 4.2810i	-0.4422 + 4.7930i	-2.8852 + 3.4939i	-0.3165 + 4.1393i	-3.0040 + 4.3719i
-0.5102 + 4.5222i	-0.4262 + 4.6307i	-0.5540 + 4.6058i	-0.4343 + 4.6279i	-1.7355 + 4.3290i	-0.4257 + 4.6304i	-3.8647 + 3.1091i
-0.5138 + 4.5350i	-0.7587 + 4.8221i	-0.3853 + 4.1037i	-0.8799 + 4.8280i	-0.5570 + 4.5942i	-0.8761 + 4.8356i	-0.6334 + 4.5714i
				-0.3915 + 4.0929i		-0.4360 + 4.0779i

TABLE 13. Local eigenvalue system.

No PSS (pu) 1.0e+02	PSO		FA		MOA	
	PSS1A (pu) 1.0e+02	PSS2B (pu) 1.0e+02	PSS1A (pu) 1.0e+02	PSS2B (pu) 1.0e+02	PSS1A (pu) 1.0e+02	PSS2B (pu) 1.0e+02
-1.0213 + 9.0136i	-1.0317 + 9.1858i	-1.1949 + 8.9039i	-1.0260 + 9.0958i	-1.1907 + 8.9167i	-1.0309 + 9.1684i	-1.2091 + 8.9756i
-0.9048 + 7.9630i	-1.0200 + 8.2822i	-2.8381 + 6.5373i	-0.9895 + 8.1422i	-2.8933 + 6.4799i	-1.0211 + 8.2608i	0.5610 + 6.5499i
-1.0649 + 7.0789i	-1.2117 + 7.0760i	-0.5425 + 6.7395i	-1.2041 + 7.0987i	-0.5409 + 6.7030i	-1.1923 + 7.1393i	-3.4840 + 6.4998i
-0.8536 + 6.8864i	-0.7892 + 6.4807i	-3.1400 + 5.4015i	-0.9887 + 6.5583i	-1.6124 + 6.3038i	-0.9749 + 6.5533i	-1.8207 + 6.4342i
-1.4630 + 6.2015i	-1.4899 + 6.2543i	-1.6166 + 6.3042i	-1.4602 + 6.2401i	-1.1746 + 5.8501i	-1.4845 + 6.2640i	-2.2284 + 5.6225i
-1.0967 + 5.8258i	-1.4695 + 5.9501i	-1.6983 + 5.8658i	-1.4333 + 5.9742i	-1.7084 + 5.8717i	-1.3885 + 6.0100i	-1.2537 + 5.8688i
-0.7855 + 5.3365i	-1.3383 + 5.9045i	-1.1919 + 5.8246i	-1.4008 + 5.8759i	-0.9637 + 5.4750i	-1.4194 + 5.8719i	-1.3045 + 5.3270i
-1.2478 + 5.8277i	-1.2545 + 5.7240i	-1.2160 + 5.5320i	-0.9218 + 5.6602i	-0.9255 + 5.3628i	-0.9239 + 5.6637i	-1.0081 + 5.5210i
-0.9336 + 5.5105i	-0.9388 + 5.6631i	-0.9220 + 5.3572i	-0.8167 + 5.3654i	-1.2543 + 5.3615i	-0.8145 + 5.3731i	-0.9841 + 5.4001i
-0.9910 + 5.4659i	-1.1367 + 5.6708i	-0.9812 + 5.4927i	-1.1556 + 5.6853i	-1.2345 + 5.5216i	-1.2344 + 5.7325i	-0.9941 + 5.4502i
-1.1518 + 5.6620i	-0.8159 + 5.3669i	-0.9971 + 5.4622i	-1.1398 + 5.6662i	-0.9980 + 5.4613i	-1.1397 + 5.6804i	-1.4311 + 5.0707i
-1.1491 + 5.6578i	-1.0009 + 5.4744i	-1.2931 + 5.3585i	-0.9934 + 5.4774i		-0.9941 + 5.4773i	

the aim was to observe an increase in system damping, which contributes to enhanced stability in the Sulselrabar system.

The objective function utilized in this study was to maximize the minimum damping (ζ_{min}) in the system. Once the optimal placement of the PSS is determined based on the damping values associated with each PSS placement probability, the system response can be observed and analyzed. This includes an evaluation of the Velocity Deviation ($\Delta\omega$),

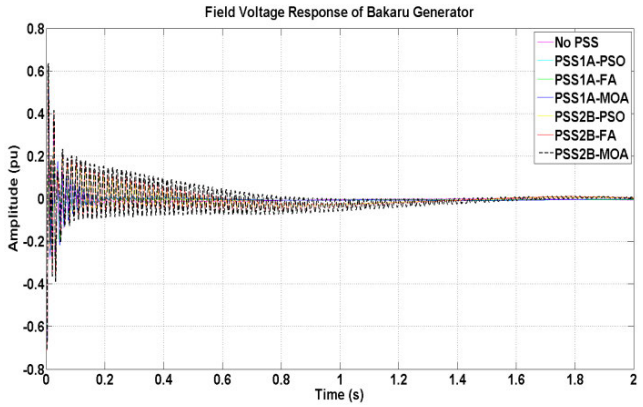

FIGURE 14. Field voltage response (E_{fd}) of Bakaru generator.

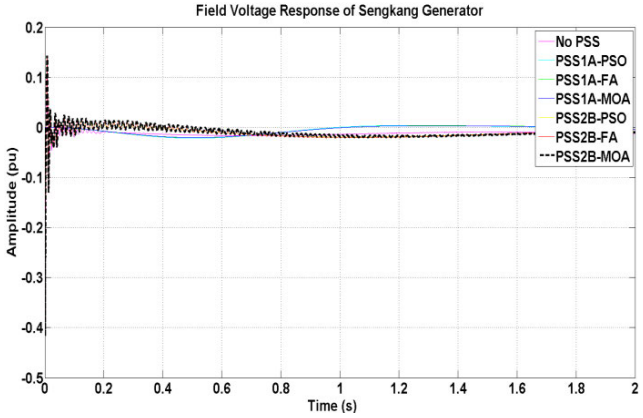

FIGURE 15. Field voltage response (E_{fd}) of Sengkang generator.

Field Voltage Response (E_{fd}), and rotor angle response of each generator. In addition, this study includes an analysis of the eigenvalues and overshoots of each generator. The linear model of the system is subjected to a disturbance input, specifically a change in load demand of 0.05 pu applied to the BAKARU and SENGKANG Generators. This load change leads to a situation in which the mechanical power input (Pm) becomes less than the electrical power output (Pe), resulting in a decrease in the response of the angular velocity (ω) of the generator.

The PSS placement index was evaluated using the Mayfly Optimization Algorithm (MOA) as the proposed method. In addition to MOA, the Firefly Algorithm (FA) and Particle Swarm Optimization (PSO) methods were used for comparison during the evaluation process. This evaluation was likely aimed at comparing the effectiveness of these three methods in determining the PSS placement index. The priority for PSS placement is based on the maximum value of ζ_{min}, which is considered more significant than ζ_0. Fig. 10 presents a comparison of the placement indices for the priority locations designated for installing PSS. This may provide a visual representation of how the placement index varies for each location based on the minimum damping eigensystem of each installation scheme.

After adding the PSS, the damping values of the system increased. It was observed that the MB-PSS2B method yields a superior damping system compared to the PSS1A method. For example, when utilizing the MOA method, the maximum damping value achieved with PSS1A was 0.589421505, whereas that with MB-PSS2B was 0.722521481. A good damping value for the system is considered greater than 0.1, indicating that the system is in a stable condition and can effectively dampen oscillations. Table 5-6 likely present the results of the PSS parameter tuning, which demonstrate the specific parameter values achieved through the optimization process.

1) TIME DOMAIN SIMULATION

In this section, we focus on the stability of the system in the presence of disturbances on Bus 1 (BAKARU generator) and Bus 13 (SENGKANG generator). The BAKARU generator is one of the largest generators in the Sulselrabar system with an installed power capacity of 126 MW. Owing to its substantial capacity and adaptive capabilities, the BAKARU generator is considered a swing generator in the system. On the other hand, the SENGKANG generator is the largest generator in the Sulselrabar system, with an installed power capacity of 192 MW. It is a gas and steam-type thermal generator. Fig. 11 and 12 depict the speed responses of the BAKARU and SENGKANG generators, respectively, when a disturbance occured at buses 1 and 13. These figures provide insights into how the speed of each generator is affected by disturbances at their respective buses.

When a change in the load occurs, the mechanical power (Pm) is less than the electrical power (Pe), and the speed (ω) of the generator initially responds by decreasing. The role of the control equipment is crucial for maintaining generator stability under such conditions. In a system without additional control, the performance of the exciter is limited, leading to oscillating speed responses, as shown in Fig. 11. Fig. 11 shows the speed response of the generator without additional control, where the oscillations range from -0.0204 pu to 0.004468 pu. However, after installing the PSS1A control, an improvement in performance was observed, with a reduced overshoot ranging from -0.01623 pu to 0.002111 pu. The combination of the system with PSS2B yielded an even more optimal performance, with a slight oscillation range of -0.01183 pu to 0.0007239 pu. Similarly, Fig. 12 shows the response of the SENGKANG generator. Without additional control, the system exhibited an overshoot ranging from -0.02218 pu to 0.00455 pu. With the inclusion of PSS1A, there was an improvement in the overshoot, which ranged from -0.02054 pu to 0.003083 pu. The use of PSS2B further enhanced the performance, resulting in a more optimal overshoot range of -0.01279 pu to 0.0009203 pu. Comparing the proposed MOA-based method with the FA and PSO methods, the MOA method demonstrated optimal results, with lower overshoot values. This indicates that the MOA-based approach is more effective in achieving an improved generator performance. Table 8 presents the speed deviations of all

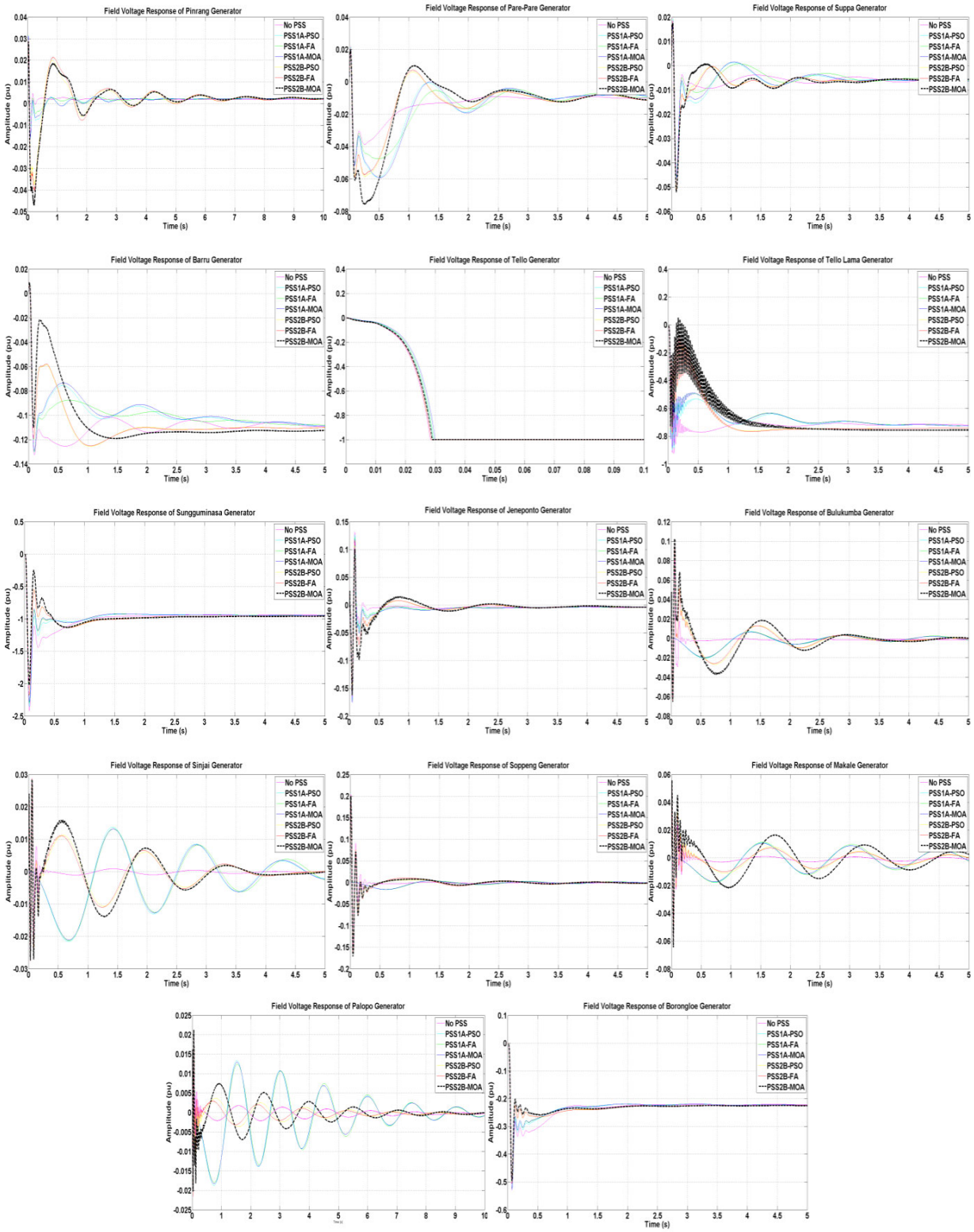

FIGURE 16. Field voltage response (E_{fd}) of all generator.

the generators, providing a comprehensive overview of the deviations for each generator.

Table 8 presents a comparison of the response speed of the Sulselrabar generator system when a disturbance occurs in the form of a change in the load on buses 1 and 13. The table compares various control schemes, and the minimum overshoot deviation was observed in the system with a control scheme based on PSS2B, which was optimized using

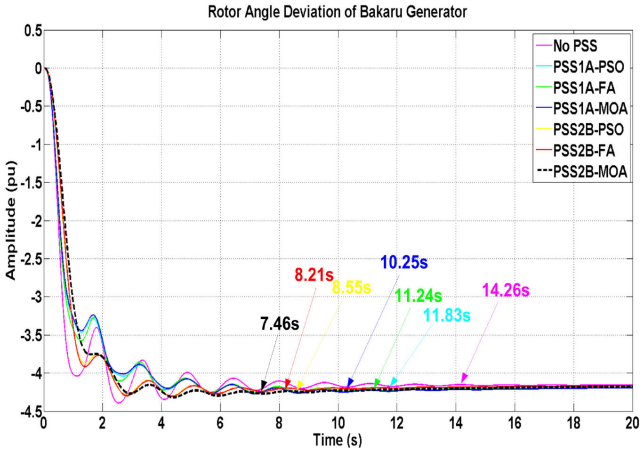

FIGURE 17. Rotor angle deviation of Bakaru generator.

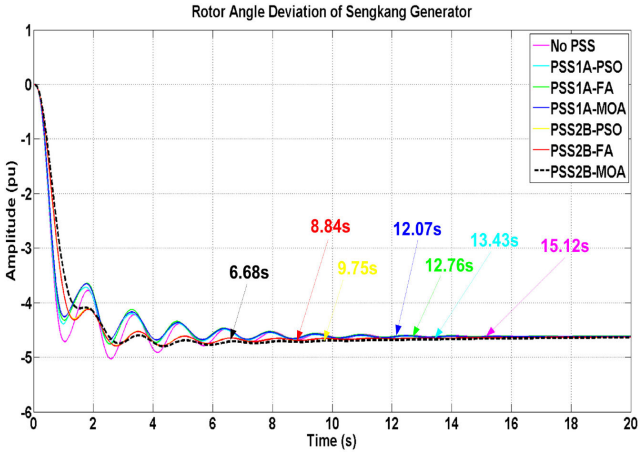

FIGURE 18. Rotor angle deviation of Sengkang generator.

the MOA method. This indicates that generator performance is optimal when additional PSS controls are installed. The improvement in generator performance can be attributed to the limitations of the exciter equipment in providing control signals, specifically the Field Voltage, to the generator.

By installing a PSS, the control signals and response of the field voltage can be enhanced, leading to improved generator behavior during disturbances. Fig. 14 and 15 illustrate the response of the BAKARU and SENGKANG generator field voltages, respectively, when a disturbance occurs. These figures provide visual representations of the response of the field voltage of each generator to the disturbances. Indeed, the MOA method demonstrated favorable response results compared with the FA and PSO methods.

The superior performance of the MOA method indicates its effectiveness in improving the system stability and control. Fig. 16 shows the field voltage responses of the other generators in the system when subjected to disturbances. This provides a visual representation of how the field voltage of each generator responds under given conditions. Table 9 presents additional details regarding the field-voltage responses of the generators. It can provide specific values or metrics related to the field voltage response, such as overshoot, damping, or other relevant parameters. This table can help to evaluate the performance and effectiveness of each control scheme.

The generator stability performance can be assessed by analyzing the rotor angle response of the generators. Fig. 17 and 18 illustrate the angular deviation responses of the BAKARU and SENGKANG generator rotors, respectively, when disturbances occur at buses 1 and 13. These figures provide insight into how the rotor angles of the generators are affected by disturbances. Fig. 19 shows the rotor angle responses of the other generators in the system when subjected to the same disturbances. By comparing the rotor angle responses, it is possible to observe the impact of additional controls on generator oscillations and settling time. Generators without additional controls often exhibit pronounced oscillations and long settling times. This emphasizes the importance of implementing additional controls, such as PSS, to enhance the stability and response of the generators during disturbances.

The MOA-based optimization method demonstrated optimal results compared with the FA and PSO methods. In Fig. 17, it can be observed that the BAKARU generator without additional control has a settling time of 14.26 seconds. However, with the implementation of PSS1A, the settling time improves to 10.25 seconds, and with PSS2B, it was further reduced to 7.46 s. This indicates that the inclusion of PSS2B resulted in a faster settling time for the BAKARU generator. Similarly, as shown in Fig. 18, the SENGKANG generator without additional control exhibits a settling time of 15.12 seconds. With PSS1A, the settling time decreases to 12.07 seconds, and with PSS2B, it further improved to 6.692 s. These results highlight the effectiveness of PSS2B in achieving a significantly shorter settling time for the SENGKANG generator. Table 10 presents a comparison of the settling times of the generators under the various control schemes. This table allows for a more comprehensive assessment of settling time performance across different control methods.

2) EIGENVALUE ANALYSIS

This section focuses on the analysis of eigenvalue systems for systems without PSS, PSS1A, and PSS2B. The analysis included the critical eigenvalues (Table 11), eigenvalues of the inter-area system (Table 12), and eigenvalues of the local system (Table 13). These tables provide insights into the behavior of eigenvalue systems under different control schemes. In general, the tables demonstrate an improvement in the eigenvalue system with the implementation of the various control schemes. This improvement is indicated by the position of the eigenvalues, which tend to shift towards the left, and the real part (σ), which becomes more negative. A more negative real part implies improved stability of the system. Specifically, the Multi-Band PSS type PSS2B is effective in enhancing the eigenvalue and damping system. This is evident from the more negative eigenvalues shown in

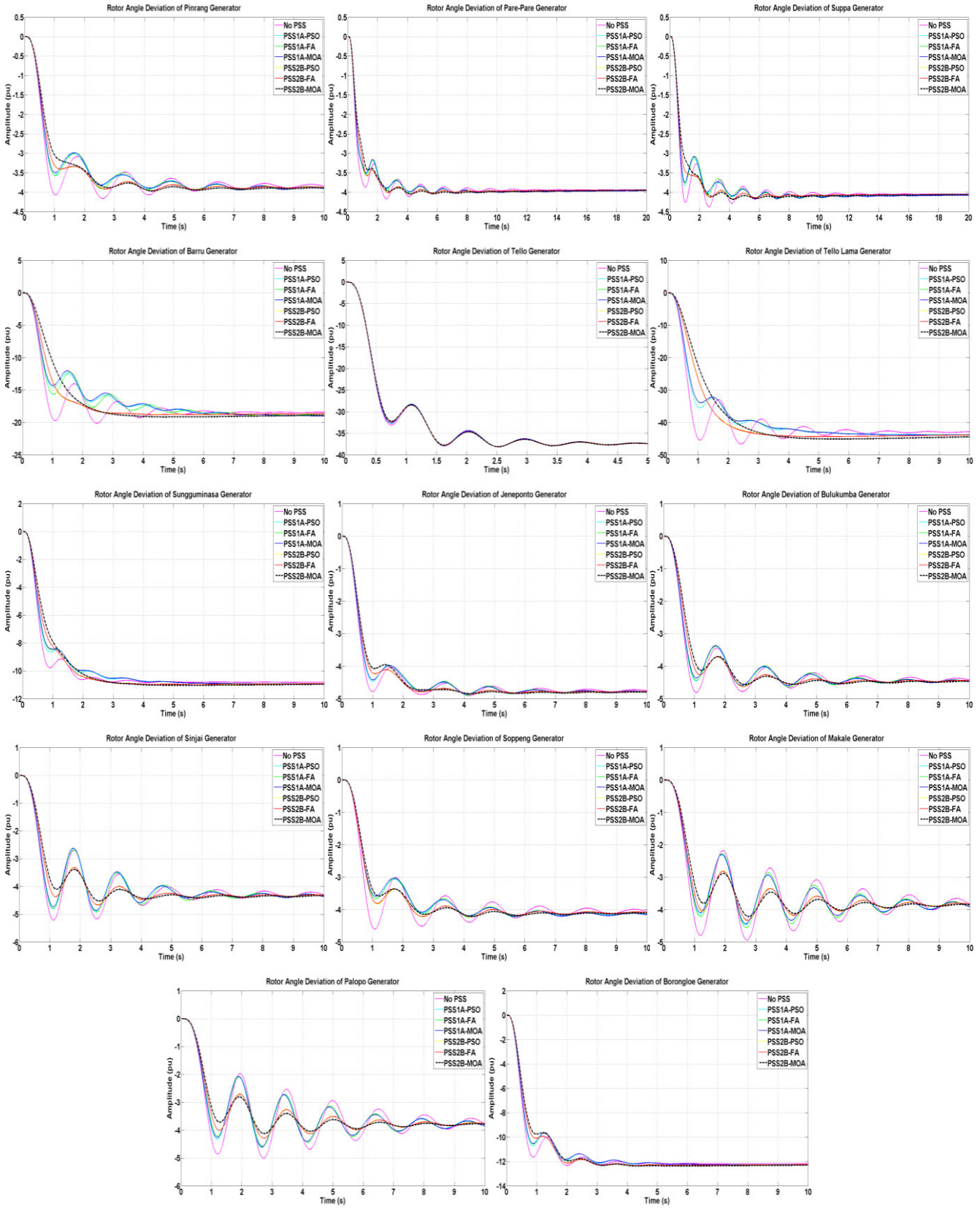

FIGURE 19. Rotor angle deviation of all generator.

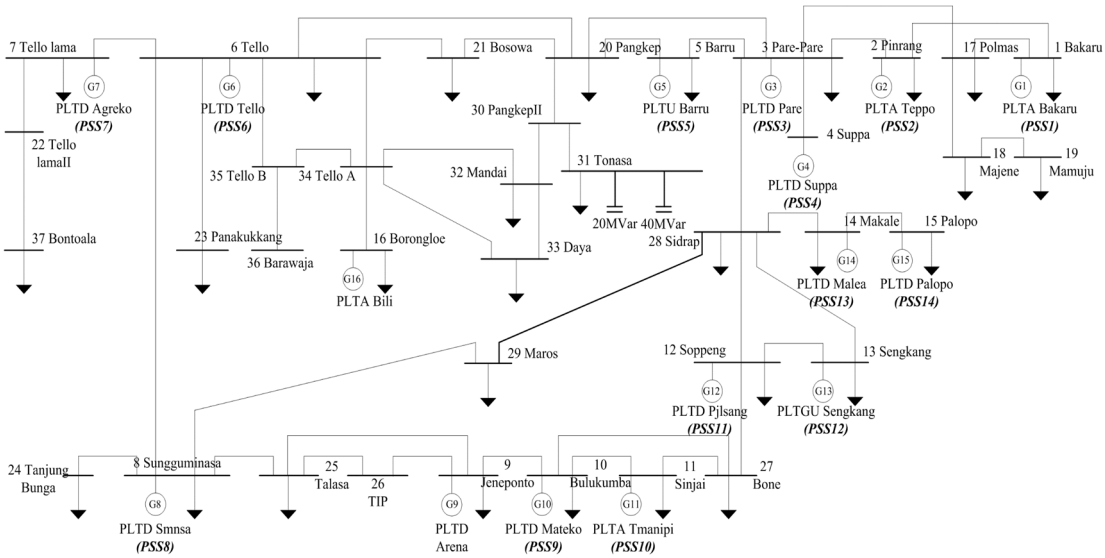

FIGURE 20. Single line diagram Sulselrabar system after optimization.

the table. The improved eigenvalues contribute to the overall stability and performance of a system.

The load changes result in the electric power (Pe) being greater than the mechanical power (Pm), leading to a downward response in the generator speed when a disturbance occurs. Simultaneously, because $Pe > Pm$, the rotor decelerates, resulting in a negative rotor angle response. These disturbances were observed in the BAKARU and SENGKANG generators, which are the largest electricity producers in Sulselrabar. The overshoot oscillations were reduced by installing the PSS, indicating an improvement in the stability of the Sulselrabar system. MB-PSS2B provides the maximum damping to the system, further enhancing its stability. Moreover, the settling time, which is the time required for the system to reach steady-state conditions, was improved with the proposed control scheme based on MB-PSS2B using the MOA method. The reduced settling time signifies a faster response and attainment of steady-state conditions. Overall, the use of PSS, particularly MB-PSS2B optimized with the MOA method, resulted in increased stability, reduced overshoot oscillations, and a faster settling time in the Sulselrabar system.

Fig. 20 illustrates the single-line diagram system of Sulselrabar after optimizing the placement of SVC and MB-PSS2B using the MOA method. This optimized configuration ensures the optimal placement of the SVC and MB-PSS2B within the Sulselrabar electric power system. The optimal placement and tuning of SVC equipment in an electric power system serves several important functions. First, the SVC can compensate for reactive power losses, which helps improve the overall power factor and reduce energy losses in the system. By injecting or absorbing reactive power as required, the SVC helps maintain the desired voltage profile and improves the system efficiency. Furthermore, the SVC plays a crucial role in regulating the voltage, especially during variations in the load demand and system conditions. By dynamically adjusting the reactive power output, the SVC helps stabilize and regulate the system voltage levels within acceptable limits, thereby ensuring proper voltage stability throughout the system. The optimal placement and tuning of the SVC equipment also contributeds to increased system operational safety. By addressing reactive power issues, controlling voltage levels, and improving system stability, SVC enhance the overall reliability and security of electric power systems. Reactive power plays a vital role in maintaining the voltage stability in all-electric power transmission systems. Proper management and control of reactive power facilitated by SVC helps ensure voltage stability and mitigates voltage fluctuations, voltage collapse, and other potential stability issues.

V. CONCLUSION

This research proposes the optimization of the location and optimal parameters of the SVC and MB-PSS2B in the Sulselrabar system based on the MOA. From the SVC optimization results, the optimal location for installing an SVC on bus 31 is 40 MW, resulting in an improvement in the bus voltage profile, increased operational security limits of the system, and a reduction in losses by 0.19 MW. Meanwhile, the optimal location for installing MB-PSS2B is on 14 generators with parameters optimized using the MOA method. The application of MB-PSS2B based on MOA provided optimal results compared with the other control schemes. This was evidenced by the minimal overshoot oscillation, fast settling time, optimal response of the generator field voltage, and improved eigenvalues of the system. An improvement in the system stability was also observed with an increase in the damping ratio. The installation of 14 MOA-based MB-PSS2B units yielded the highest damping ratio compared with the other control schemes, specifically at 0.722521481.

In this study, MOA was used to optimize SVC and MB-PSS2B. As a comparative method, our previous work utilized the FA and PSO. In the FA method, the resulting

fitness function value was 75.43756268, and convergence was achieved at the 22nd iteration. The PSO method produced a fitness function value of 75.73499109 at the 39th iteration. In contrast, the method proposed by the MOA showed a minimum fitness function value of 75.1222 at the 16th iteration. These results indicate that the MOA method produces a minimum fitness function value with a faster computational process than the FA and PSO methods.

The use of MOA to optimize SVC and MB-PSS can be considered in future work to improve the stability of a multimachine system with integrated solar and wind hybrid powers.

REFERENCES

[1] M. Y. Yunus, M. R. Djalal, and M. Marhatang, "Optimal design power system stabilizer using firefly algorithm in interconnected 150 kV Sulselrabar system, Indonesia," *Int. Rev. Electr. Eng.*, vol. 12, no. 3, p. 250, Jun. 2017, doi: 10.15866/iree.v12i3.11136.

[2] Y. Tang, *Voltage Stability Analysis of Power System*. Cham, Switzerland: Springer, 2021.

[3] R. F. Mochamad, R. Preece, and K. N. Hasan, "Probabilistic multi-stability operational boundaries in power systems with high penetration of power electronics," *Int. J. Electr. Power Energy Syst.*, vol. 135, Feb. 2022, Art. no. 107382, doi: 10.1016/j.ijepes.2021.107382.

[4] P. Dey, C. Sumpavakup, and P. Kirawanich, "Optimal control of grid connected electric railways to mitigate low frequency oscillations," in *Proc. Res., Invention, Innov. Congr., Innov. Elect. Electron.*, 2022, pp. 70–75, doi: 10.1109/RI2C56397.2022.9910283.

[5] M. S. Aziz and A. G. Abdullah, "Hybrid control strategies of SVC for reactive power compensation," *Indonesian J. Electr. Eng. Comput. Sci.*, vol. 19, no. 2, pp. 563–571, 2020, doi: 10.11591/ijeecs.v19.i2.pp563-571.

[6] R. Fazal and M. A. Choudhry, "Design of non-linear static VAR compensator based on synergetic control theory," *Electr. Power Syst. Res.*, vol. 151, pp. 243–250, Oct. 2017, doi: 10.1016/j.epsr.2017.05.014.

[7] S. R. Paital, P. K. Ray, A. Mohanty, and S. Dash, "Stability improvement in solar PV integrated power system using quasi-differential search optimized SVC controller," *Optik*, vol. 170, pp. 420–430, Oct. 2018, doi: 10.1016/j.ijleo.2018.05.097.

[8] P. Dey, A. Bhattacharya, and P. Das, "Tuning of power system stabilizer for small signal stability improvement of interconnected power system," *Appl. Comput. Informat.*, vol. 16, no. 1/2, pp. 3–28, Dec. 2017, doi: 10.1016/j.aci.2017.12.004.

[9] P. K. Ray, S. R. Paital, A. Mohanty, F. Y. S. Eddy, and H. B. Gooi, "A robust power system stabilizer for enhancement of stability in power system using adaptive fuzzy sliding mode control," *Appl. Soft Comput.*, vol. 73, pp. 471–481, Dec. 2018, doi: 10.1016/j.asoc.2018.08.033.

[10] P. Dey, A. Saha, A. Bhattacharya, and B. Marungsri, "Analysis of the effects of PSS and renewable integration to an inter-area power network to improve small signal stability," *J. Electr. Eng. Technol.*, vol. 15, no. 5, pp. 2057–2077, Sep. 2020, doi: 10.1007/s42835-020-00499-2.

[11] M. Ravindrababu, G. Saraswathi, and K. Sudha, "Design of UPFC-PSS using firefly algorithm for stability improvement of multi machine system under contingency," *Majlesi J. Electr. Eng.*, vol. 13, no. 2, pp. 21–39, 2019.

[12] M. M. Eladany, A. A. Eldesouky, and A. A. Sallam, "Power system transient stability: An algorithm for assessment and enhancement based on catastrophe theory and FACTS devices," *IEEE Access*, vol. 6, pp. 26424–26437, 2018, doi: 10.1109/ACCESS.2018.2834906.

[13] S. U. Kakaiya, O. Cephas, G. N. Paichaure, and B. R. Parekh, "Enhancement of power system stability using FACTS devices," *Int. J. Comput. Sci. Eng.*, vol. 6, no. 12, pp. 542–546, Dec. 2018, doi: 10.26438/ijcse/v6i12.542546.

[14] J. Bhukya and V. Mahajan, "Optimization of controllers parameters for damping local area oscillation to enhance the stability of an interconnected system with wind farm," *Int. J. Electr. Power Energy Syst.*, vol. 119, Jul. 2020, Art. no. 105877, doi: 10.1016/j.ijepes.2020.105877.

[15] W. Peres and N. N. da Costa, "Comparing strategies to damp electromechanical oscillations through STATCOM with multi-band controller," *ISA Trans.*, vol. 107, pp. 256–269, Dec. 2020, doi: 10.1016/j.isatra.2020.08.005.

[16] O. M. Benaissa, S. Hadjeri, and S. A. Zidi, "Impact of PSS and SVC on the power system transient stability," in *Proc. 8th Int. Conf. Modeling, Identificat. Control (ICMIC)*, Nov. 2016, pp. 303–307, doi: 10.1109/ICMIC.2016.7804127.

[17] S. S. Bhole and P. Nigam, "Improvement of voltage stability in power system by using SVC and STATCOM," *Int. J. Adv. Res. Electr., Electron. Instrum. Eng.*, vol. 4, no. 2, pp. 749–755, Feb. 2015, doi: 10.15662/ijareeie.2015.0402035.

[18] P. Dey, S. Mitra, A. Bhattacharya, and P. Das, "Comparative study of the effects of SVC and TCSC on the small signal stability of a power system with renewables," *J. Renew. Sustain. Energy*, vol. 11, no. 3, May 2019, Art. no. 033305, doi: 10.1063/1.5085066.

[19] M. R. Shakarami and I. F. Davoudkhani, "Wide-area power system stabilizer design based on grey wolf optimization algorithm considering the time delay," *Electr. Power Syst. Res.*, vol. 133, pp. 149–159, Apr. 2016, doi: 10.1016/j.epsr.2015.12.019.

[20] Y. Welhazi, T. Guesmi, B. M. Alshammari, K. Alqunun, A. Alateeq, Y. Almalaq, R. Alsabhan, and H. H. Abdallah, "A novel hybrid chaotic Jaya and sequential quadratic programming method for robust design of power system stabilizers and static VAR compensator," *Energies*, vol. 15, no. 3, p. 860, Jan. 2022, doi: 10.3390/en15030860.

[21] B. Dasu, M. Siva Kumar, and R. Srinivasa Rao, "Design of robust modified power system stabilizer for dynamic stability improvement using particle swarm optimization technique," *Ain Shams Eng. J.*, vol. 10, no. 4, pp. 769–783, Dec. 2019, doi: 10.1016/j.asej.2019.07.002.

[22] A. Khodabakhshian and R. Hemmati, "Multi-machine power system stabilizer design by using cultural algorithms," *Int. J. Electr. Power Energy Syst.*, vol. 44, no. 1, pp. 571–580, Jan. 2013, doi: 10.1016/j.ijepes.2012.07.049.

[23] Z. Seddiki, T. Allaoui, M. Bey, and M. Denai, "Combining multi-band power system stabilizers and hybrid power flow controllers to support electricity grids with high penetration of distributed renewable generation," *Indonesian J. Electr. Eng. Informat.*, vol. 10, no. 2, pp. 441–451, May 2022, doi: 10.52549/ijeei.v10i2.3666.

[24] *IEEE Recommended Practice for Excitation System Models for Power System Stability Studies*, IEEE Standard 421.5-2016, 2016, pp. 1–207, doi: 10.1109/IEEESTD.2006.99499.

[25] M. Fan, K. Wang, and J. Zhang, "Parameters setting of power system stabilizer PSS2B," in *Proc. 4th Int. Conf. Renew. Energy Environ. Technol.*, 2017, pp. 63–70, doi: 10.2991/icreet-16.2017.12.

[26] A. A. Alsakati, C. A. Vaithilingam, J. Alnasseir, K. Naidu, and G. Rajendran, "Transient stability enhancement of grid integrated wind energy using particle swarm optimization based multi-band PSS4C," *IEEE Access*, vol. 10, pp. 20860–20874, 2022, doi: 10.1109/ACCESS.2022.3151425.

[27] W. Huang and K. Sun, "Optimization of SVC settings to improve post-fault voltage recovery and angular stability," *J. Mod. Power Syst. Clean Energy*, vol. 7, no. 3, pp. 491–499, May 2019, doi: 10.1007/s40565-018-0479-0.

[28] H. Merah, A. Gacem, D. Ben Attous, A. Lashab, F. Jurado, and M. A. Sameh, "Sizing and sitting of static VAR compensator (SVC) using hybrid optimization of combined cuckoo search (CS) and antlion optimization (ALO) algorithms," *Energies*, vol. 15, no. 13, p. 4852, Jul. 2022, doi: 10.3390/en15134852.

[29] A. Naderipour, Z. Abdul-Malek, F. H. Gandoman, S. A. Nowdeh, M. A. Shiran, M. J. H. Moghaddam, and I. F. Davoodkhani, "Optimal designing of static VAR compensator to improve voltage profile of power system using fuzzy logic control," *Energy*, vol. 192, Feb. 2020, Art. no. 116665, doi: 10.1016/j.energy.2019.116665.

[30] M. Ĉalasan, T. Konjić, K. Kecojević, and L. Nikitović, "Optimal allocation of static VAR compensators in electric power systems," *Energies*, vol. 13, no. 12, p. 3219, Jun. 2020, doi: 10.3390/en13123219.

[31] T. Hussein, "Performance of power system stabilizer (UNITROL D) in Benghazi north power plant," *Int. J. Electr. Comput. Eng.*, vol. 5, no. 2, pp. 221–224, 2011, doi: 10.5281/zenodo.1057566.

[32] A. A. Alsakati, C. A. Vaithilingam, K. Naidu, G. Rajendran, J. Alnasseir, and A. Jagadeeshwaran, "Particle swarm optimization for tuning power system stabilizer towards transient stability improvement in power system network," in *Proc. IEEE Int. Conf. Artif. Intell. Eng. Technol. (IICAIET)*, Sep. 2021, pp. 1–6, doi: 10.1109/IICAIET51634.2021.9573534.

[33] P. Marić, R. Kljajić, H. R. Chamorro, and H. Glavaš, "Power system stabilizer tuning algorithm in a multimachine system based on S-domain and time domain system performance measures," *Energies*, vol. 14, no. 18, p. 5644, Sep. 2021, doi: 10.3390/en14185644.

[34] J. Morsali, "TID-based PSS2B to overcome LFO issue in multi-machine power systems," in *Proc. 30th Int. Conf. Electr. Eng.*, May 2022, pp. 968–973, doi: 10.1109/ICEE55646.2022.9827003.
[35] W. Peres, F. C. R. Coelho, and J. N. N. Costa, "A pole placement approach for multi-band power system stabilizer tuning," *Int. Trans. Electr. Energy Syst.*, vol. 30, no. 10, pp. 1–10, Oct. 2020, doi: 10.1002/2050-7038.12548.
[36] A. A. Alsakati, C. A. Vaithilingam, J. Alnasseir, and A. Jagadeeshwaran, "Investigation of single-band and multi-band power system stabilizers towards transient stability improvement in electrical networks," in *Proc. IEEE Conf. Energy Convers. (CENCON)*, Oct. 2021, pp. 196–201, doi: 10.1109/CENCON51869.2021.9627246.
[37] A. Shankar Kar and G. Gurrala, "A systematic tuning approach for multi-band power system stabilizers (PSS4B)," in *Proc. Int. Symp. Power Electron., Electr. Drives, Autom. Motion (SPEEDAM)*, Jun. 2020, pp. 628–633, doi: 10.1109/SPEEDAM48782.2020.9161835.
[38] S. Mitra, A. Bhattacharya, and P. Dey, "Small signal stability analysis in co-ordination with PSS, TCSC, and SVC," in *Proc. Int. Conf. Comput. Power, Energy, Inf. Commun. (ICCPEIC)*, Mar. 2018, pp. 434–441, doi: 10.1109/ICCPEIC.2018.8525148.
[39] M. Eslami, H. Shareef, A. Mohamed, and M. Khajehzadeh, "Coordinated design of PSS and SVC damping controller using CPSO," in *Proc. 5th Int. Power Eng. Optim. Conf.*, Jun. 2011, pp. 11–16, doi: 10.1109/PEOCO.2011.5970394.
[40] N. A. M. Kamari, I. Musirin, and A. A. Ibrahim, "Swarm intelligence approach for angle stability improvement of PSS and SVC-based SMIB," *J. Electr. Eng. Technol.*, vol. 15, no. 3, pp. 1001–1014, May 2020, doi: 10.1007/s42835-020-00386-w.
[41] J. Ansari, A. R. Abbasi, M. H. Heydari, and Z. Avazzadeh, "Simultaneous design of fuzzy PSS and fuzzy STATCOM controllers for power system stability enhancement," *Alexandria Eng. J.*, vol. 61, no. 4, pp. 2841–2850, Apr. 2022, doi: 10.1016/j.aej.2021.08.007.
[42] M. Djalal, "Optimal power system stabilizer design using craziness particle swarm optimization in Sulselrabar system," *Przegląd Elektrotechniczny*, vol. 1, no. 10, pp. 78–83, Sep. 2021, doi: 10.15199/48.2021.10.15.
[43] K. Zervoudakis and S. Tsafarakis, "A mayfly optimization algorithm," *Comput. Ind. Eng.*, vol. 145, Jul. 2020, Art. no. 106559, doi: 10.1016/j.cie.2020.106559.
[44] E. V. Fortes, L. F. B. Martins, M. V. S. Costa, L. Carvalho, L. H. Macedo, and R. Romero, "Mayfly optimization algorithm applied to the design of PSS and SSSC-POD controllers for damping low-frequency oscillations in power systems," *Int. Trans. Electr. Energy Syst.*, vol. 2022, Apr. 2022, Art. no. 5612334, doi: 10.1155/2022/5612334.
[45] A. A. Eid, A. M. A. Soliman, and M. A. Mehanna, "Optimize gain values of PI-controller for active power filter using mayfly algorithm," *Int. J. Renew. Energy Res.*, vol. 12, no. 4, pp. 1727–1735, 2022, doi: 10.20508/ijrer.v12i4.13413.g8597.
[46] G. Lei, X. Chang, Y. Tianhang, and W. Tuerxun, "An improved mayfly optimization algorithm based on median position and its application in the optimization of PID parameters of hydro-turbine governor," *IEEE Access*, vol. 10, pp. 36335–36349, 2022, doi: 10.1109/ACCESS.2022.3160714.
[47] L. A. Ordaz-Padilla, R. Peña-Gallardo, and J. A. Morales-Saldaña, "Robust stability analysis for a power system stabilizer," in *Proc. 13th Int. Conf. Power Electron. (CIEP)*, Jun. 2016, pp. 345–349, doi: 10.1109/CIEP.2016.7530782.
[48] H. Setiadi, N. Mithulananthan, R. Shah, M. R. Islam, A. Fekih, A. U. Krismanto, and M. Abdillah, "Multi-mode damping control approach for the optimal resilience of renewable-rich power systems," *Energies*, vol. 15, no. 9, p. 2972, Apr. 2022, doi: 10.3390/en15092972.
[49] H. Saadat, *Power System Analysis*. New York, NY, USA: McGraw-Hill, 2009.
[50] P. S. Kundur and O. P. Malik, *Power System Stability and Control*. New York, NY, USA: McGraw-Hill, 2022.
[51] H. Setiadi, F. Arrazi, M. Abdillah, and A. U. Krismanto, "Smart DIPSS for dynamic stability enchancement on multi-machine power system," *Indonesian J. Electr. Eng. Informat.*, vol. 10, no. 1, pp. 43–50, Mar. 2022, doi: 10.52549/ijeei.v10i1.3429.
[52] I. Manuaba, U. Udayana, M. Abdillah, R. Zamora, H. Setiadi, U. Pertamina, and U. Airlangga, "Adaptive power system stabilizer using kernel extreme learning machine," *Int. J. Intell. Eng. Syst.*, vol. 14, no. 3, pp. 468–480, Jun. 2021, doi: 10.22266/ijies2021.0630.39.
[53] E. A. Belati, C. F. Nascimento, H. de Faria, E. H. Watanabe, and A. Padilha-Feltrin, "Allocation of static VAR compensator in electric power systems considering different load levels," *J. Control, Autom. Electr. Syst.*, vol. 30, no. 1, pp. 1–8, Feb. 2019, doi: 10.1007/s40313-018-00421-2.
[54] Q. Lu, Y. Sun, and S. Mei, "Nonlinear control of static VAR systems," in *Nonlinear Control Systems and Power System Dynamics*, Q. Lu, Y. Sun, and S. Mei, Eds. Boston, MA, USA: Springer, 2001, pp. 309–342, doi: 10.1007/978-1-4757-3312-9_9.
[55] M. Priyadhershni, C. Udhayashankar, and V. K. Chinnaiyan, "Simulation of static VAR compensator in IEEE 14 bus system for enhancing voltage stability and compensation," in *Power Electronics and Renewable Energy Systems*. New Delhi, India: Springer, 2015, pp. 265–273, doi: 10.1007/978-81-322-2119-7_27.
[56] Z.-M. Gao, J. Zhao, S.-R. Li, and Y.-R. Hu, "The improved mayfly optimization algorithm," *J. Phys., Conf. Ser.*, vol. 1684, no. 1, Nov. 2020, Art. no. 012077, doi: 10.1088/1742-6596/1684/1/012077.

MUHAMMAD RUSWANDI DJALAL was born in Ujung Pandang, in March 1990. He received the bachelor's degree in energy engineering from the State Polytechnic of Ujung Pandang, Makassar, Indonesia, in 2012, and the master's degree in electrical engineering from the Sepuluh Nopember Institute of Technology, Surabaya, Indonesia, in 2015, where he is currently pursuing the Ph.D. degree with the Department of Electrical Engineering. He is a Lecturer in energy engineering with the Department of Mechanical Engineering, State Polytechnic of Ujung Pandang. His research interests include power system stability, renewable energy, and artificial intelligence (AI).

IMAM ROBANDI was born in Kebumen, in August 1963. He received the bachelor's degree in electrical engineering from the Sepuluh Nopember Institute of Technology, Surabaya, Indonesia, in 1989, the master's degree from the Department of Electrical Engineering, Bandung Institute of Technology, Bandung, Indonesia, in 1995, and the Ph.D. degree from the Department of Electrical Engineering, Totory University, Japan, in 2002. He is currently a Professor with the Department of Electrical Engineering, Sepuluh Nopember Institute of Technology. He is also the Head of the Power System Operation and Control Laboratory, Department of Electrical Engineering, Sepuluh November Institute of Technology. He specializes in the application of artificial intelligence in electrical power system engineering.

MOHAMMAD ALMAS PRAKASA was born in Brebes, in September 1999. He received the bachelor's degree in electrical engineering from Universitas Negeri Semarang, Semarang, Indonesia, in 2017, and the master's degree from the Department of Electrical Engineering, Sepuluh Nopember Institute of Technology, Surabaya, Indonesia, in 2021, where he is currently pursuing the Ph.D. degree with the Department of Electrical Engineering. He is a member of the Power System Operation and Control Laboratory. His research interests include applying artificial intelligence to electrical power systems, especially to power system stability and renewable energy.